2023-05-01

Addressing the Challenged of DCOP Based Decision-Making Algorithms in Modern Power Systems

Luis Daniel Ramirez Burgueno
University of Texas at El Paso

ADDRESSING THE CHALLENGES OF DCOPF BASED DECISION-MAKING ALGORITHMS IN MODERN POWER SYSTEMS

LUIS DANIEL RAMIREZ-BURGUENO

Master's Program in Electrical Engineering

APPROVED:

Yuanrui Sang, Ph.D., Chair

Michael McGarry, Ph.D.

Nayda Santiago, Ph.D.

Bill Tseng, Ph.D.

Stephen L. Crites, Jr., Ph.D.
Dean of the Graduate School

To my family, for their infinite love and support.

ADRESSING THE CHALLENGES OF DCOPF BASED DECISION-MAKINGALGORITHMS IN MODERN POWER SYSTEMS

by

LUIS DANIEL RAMIREZ BURGUENO, B.S.

THESIS

Presented to the Faculty of the Graduate School of

The University of Texas at El Paso

in Partial Fulfillment

of the Requirements

for the Degree of

MASTER OF SCIENCE

Electrical and Computer Engineering

THE UNIVERSITY OF TEXAS AT EL PASO

May 2023

Acknowledgements

I would like to acknowledge and deeply thank Dr. Yuanrui Sang for all the support and guiding me through my research and thesis journey. Her words of motivation and continuous wise guidance helped me to fully develop my thesis and enhance my research experience even through difficult times and challenging problems. Thank you Dr. Sang for giving me that first research opportunity and allowing me to become a part of your research team. Also, I am deeply thankful of you introducing me to the endless possibilities of power system optimization which has held me passionate about my research.

Thanks to The University of Texas at El Paso for being a second home and providing myself with challenges that helped me grow as a human and an academic. I would like to acknowledge the College of Engineering and the department of Electrical and Computer Engineering for providing support through my bachelor's and my master's degrees. Thanks to my committee member, Dr. Nayda Santiago from the University of Puerto Rico-Mayaguez, for sharing great thoughts and allowing me to help in the development of the grid resiliency project. Also, I would like to thank Dr. Michael McGarry for first introducing me into programming and for the valuable suggestions provided for my thesis. Additionally, thank you Dr. Bill Tseng for accepting being a committee member for this thesis defense. Furthermore, I would like to thank NSF for founding the research done in this thesis.

Finally, I would like my most profound thanks to my family and their endless love. Thank you, mom and dad, for continuously investing time and teaching me the values that have forged me into the person that I am today. Also, to my brother and sister, thank you for listening and supporting me to achieve my goals in every step of my life. I would also like to thank my friends

and the very special persons around my life that have always provided support, moments of happiness, and moments of reflection.

Abstract

Natural disasters have been determined as the leading cause of power outages, causing not only huge economic losses, but also the interruption of crucial welfare activities and the arise of security concerns. Because of the later, decision-making considering grid modernization, power system economics, and system resiliency has been a crucial theme in power systems' research. The need to better withstand catastrophic events and reducing the dependency of bulky generating units has propelled the development and better management of behind-the-meter generation or distributed energy resources (DERs). DERs can assist in the grid in different manners, not only by meeting energy demand goals, but also by reducing the overall system operating cost and support the global emerging environmental objectives. By being closer to the consumer or load side, DERs avoid transmission line losses and can contribute to reduced system congestion which translates in reduced operational cost, considering that two of the three pillars that affect Locational Marginal Price (LMP) are losses and congestion. Additionally, a higher power system resilience is achieved by reducing the dependency of transmission lines that can potentially fail during a contingency event. Furthermore, DERs are primarily based on Renewable Energy Sources (RESs) which contributes to diversifying the energy generation supply and reducing the grid's fuel dependency. As a consequence, DERs in the form of RESs have the potential of reducing the overall greenhouse gas (GHG) emissions. While RESs have demonstrated over the years their numerous benefits, they also inflict a big challenge to the power grid in the form of added uncertainty and power flow instability by demanding higher system flexibility and improved decision-making algorithms. To account for this induced RESs power output uncertainty and improve power system resiliency in the decision-making process, the implementation of stochastic optimization via Monte Carlo simulations has been widely and commonly used, where different probability-based scenarios are

used to account for possible profile outcomes and renewable sources uncertainty. One of the many drawbacks of employing Monte Carlo simulations is that a power system optimization problem might be solved containing a worst-case scenario which differs significantly from the actual system condition. The latter yields consequently to a higher optimal cost, caused by the system's uncertainty. As previously mentioned, RESs enhanced management can also be achieved by improving system flexibility. A well-studied power flow control technique consists of actively changing the power system transmission topology using Optimal Transmission Switching (OTS), leading to improved power flow and transmission congestion relief. The OTS problem is based on an DC Optimal Power Flow (DCOPF) algorithm with the addition of a big-M constraint to maintain problem linearity. In such big-M based algorithm, the selection of the M value can impose great computational complexity challenges; In extreme cases, an erroneous M value selection can potentially lead to numerical instability, long solving times, and even compromise problem optimality or feasibility. Therefore, the importance of selecting an appropriate M value is noticed and well known in literature. Finally, the increased penetration of RESs will demand a better use of the different generating resources across the network control areas. Regions with great solar irradiance capabilities are and will benefit from solar generation during sun hours. In the other hand, regions with great wind and tidal power capabilities might expect high power output during night hours. Furthermore, regions with must-run generation such as nuclear or hydro power need to maintain an almost constant power output to ensure power resilience and reliability. With the latter zone's descriptions, different regions with diverse capabilities and characteristics can widely benefit from neighboring entities by allowing power exchange through system interconnections. As a consequence, distributed or decentralized algorithms that are able to reliably balance and co-optimize multiple control areas while sharing minimal system information are required. This type

of algorithms optimizes not only the region's own power dispatch, but also optimize the overall interconnected regions to exploit power exchange and interconnection benefits.

This thesis will evaluate the cost effects of decision-making under uncertainty in the power system caused by wind power RESs, where a stochastic optimization mixed integer linear program (MILP) DCOPF based model employing Monte Carlo simulations is implemented. Furthermore, an evaluation of optimally choosing the big-M value for OTS is presented to describe some of the computational challenges of decision-making in the power system. Finally, a distributed consensus based DCOPF algorithm is presented to compare the resiliency impacts between centralized and decentralized decision-making mechanisms on power systems. The presented decentralized algorithm is based on the Alternating Direction Method of Multipliers (ADMM), founded on a penalty-based objective which implements the augmented Lagrangian method for constrained optimization problems.

Table of Contents

List of Tables

List of Figures

Chapter 1: Introduction

This thesis addresses some of the decision-making challenges in modern power systems with the inclusion of Distributed Energy Resources (DERs), uncertainty, flexible topology control, effects of natural disasters, and decentralized decision-making and control. The decision-making perspective considered has the objective to minimize the operational cost and analyze the effects of different optimization algorithms based on a DC Optimal Power Flow (DCOPF) algorithm. Similarly, a resiliency focus was utilized when employing a decentralized ADMM algorithm focused again in a DCOPF algorithm. In this chapter, the background and motivation will be introduced, as also the objective of the thesis and its limitations are defined. Additionally, a short summary of the upcoming chapters will be provided.

1.1 Background and Motivation

The main inspiration of this thesis is to contribute to the ongoing and continuous transformation of the power and energy system. As the environmental goals and green-house gas emission sanctions increase, many electric facilities are aiming towards a Renewable Energy Sources (RES's) oriented generation for the upcoming years. RES can contribute to this scenario by having a positive environmental and economic effect by reducing the overall emissions and the dependency on fossil fuels. In the other hand, RES such as wind power and solar generation through Photovoltaic (PV) panels impose big challenges to the electric grid that need to be urgently addressed to maintain a reliable power system operation. These challenges are based on the intermittent and chaotic behavior that they exhibit; while intermittency can be handled by allocating flexible fast ramping units or energy storage devices, the forecast uncertainty is a more complex allocation which requires coordination of the system's available resources. A direct result of RES uncertainty being incorrectly addressed is the imbalance of load and generation. In the case

of over generation, when more output from renewable energies is obtained compared to the forecast, unscheduled power flows can potentially increase the grid overall frequency and impose penalties as set by the regulatory commissions or even cause permanent damage to devices connected to the electrical grid. On the other hand, under generation has the potential of causing rolling blackouts as also decreasing the overall electrical grid frequency. Furthermore, the mentioned imbalances can lead to severe consequences such as grid islanding from an interconnection or cause cascading failures across the electrical grid. Besides the reliability aspect of RES, market prices along the grid are based on Locational Marginal Prices (LMPs) which are dependent on the congestion, losses, and energy price aspects of a specific location. That being said, it is crucial to prioritize research in congestion management of the grid as well as minimizing generation prices under uncertainty conditions. Additionally, the inclusion of big data sets or mathematically complex algorithms maintain plenty of the state-of-the art algorithms outside of the operational scope. As a result, the requirement of computationally effective algorithms has been another motivation for the work of this thesis. Finally, the increasing resiliency needs caused by increasing natural disasters and the transition from big robust generation facilities to distributed small generation units inspired a decentralized decision-making algorithm. The latter with the objective of exploding the advantages of decentralized control compared to a central command center and the upcoming trend of the expansion of electricity markets.

1.2 THESIS CONTRIBUTION

This thesis aims to discuss the current challenges and serve as a comprehensive review for some of the power system's decision-making strategies. Being uncertainty one of the main challenges of the power system; (1) A method to price uncertainty is presented based on a stochastic optimization DCOPF model to study the economic impacts and flexible ramping

requirements of the power system under wind power RES uncertainty. Furthermore, with the inclusion of RES, greater grid flexibility is required. One of the explored techniques to achieve the latter is Optimal Transmission Switching (OTS), which allows to selectively switch on or off transmission lines. In one hand, transmission switching helps alleviate congestion in the system, improve power profiles, and reduce the total operational cost. On the downside, the OTS problem is computationally challenging by the addition of the "big-M" constraint. In this thesis, (2) a penalty approach is utilized on the DCOPF algorithm to reduce the computational time of big-M OTS problems, as also to ensure its feasibility. Finally, following the future power system trends of decentralized control and generation, (3) a decentralized consensus ADMM algorithm is presented to evaluate the power system resiliency of centralized and decentralized decision making under contingency events. The consensus ADMM based algorithm was chosen due to the minimal communication requirement between adjacent regions which is a priority in terms of data security and protection.

This thesis is limited to providing an insight of some the current challenges on modern power system's decision making. The uncertainty chapter dedicated in this thesis aims to develop a strategy to price the effects of uncertainty in terms of the system's flexible ramp and energy deployment costs. The approach uses Monte Carlo simulations to represent wind variability and does not aim to use any scenario reduction techniques or evaluates other uncertainty consideration approaches or additional uncertainty variables. Furthermore, the OTS algorithm employed in chapter 4 intends to show the effects of different big-M selections and the importance of selecting an appropriate constant value. The algorithm itself consists of a two-stage optimization model in which the objective is not exhibit a decreased overall computational time, but to show de benefits that selecting an appropriate M-value has in terms of computational time. Finally, chapter 5 aims

to exclusively show the load-loss benefits of implementing a decentralized algorithms under specific conditions, this is the case of a contingency event resulting in the loss of control center communication.

1.3 Organization and Chapter Summaries

Chapter 2 provides an approach to price wind power uncertainty, which aims to provide a reference for electric facilities to mitigate the uncertainty effects. The chapter begins with a literature review of the existing uncertainty consideration techniques and models followed by an introduction to the model, simulation specifications, and obtained results. Chapter 3 proposes a model to find optimal M values for the big-M OTS problems with the goal of reducing the problem's solution time and feasibility including a literature review involving flexible topology. Finally, Chapter 4 starts with a literature review based on decentralized decision-making algorithms and later presenting a model based on distributed optimization to enable independent decision-making on adjacent regions while allowing power exchange.

Chapter 2: The Cost of Uncertainty in Power System's Decision-Making

The current search for green and sustainable energy solutions had aimed the focus of electric facilities to RES, which had provided an optimistic future with big challenges. The volatile and intermittent nature of renewable energy sources (RES) has critical impact on the electric grid. This thesis chapter aims to propose a model to quantify the impact of the uncertainty of RES on the power system operating costs in an electricity market environment considering the use of flexible ramping (FR) products, compensation for wind power curtailment, and the cost for flexible load curtailment, and thus offer a method to price the uncertainty of RES. The model is based on a stochastic optimization model for power system operations considering flexible ramping products, and the uncertainty cost is calculated by comparing the dispatch cost with and without uncertainties. The method was implemented on a modified RTS-96 test system with a high penetration of wind energy, and the uncertainty of wind power output were represented using three different distributions, namely, Gamma, Weibull, and Rayleigh. Results show that the uncertainty of wind power increases power system operating costs, and the uncertainty prices of wind power can be evaluated based on the difference of generation costs and penalty of wind power or load curtailment between the cases with and without uncertainties.

2.1 NOMENCLATURE

Indices

b	Bus.
g	Generator.
l	Transmission Line.
s	Scenario.
seg	Segments for piece-wise linear cost function.
t	Time.
w	Wind farms.
ϕ	Distribution Type.

Sets

NL_b^+	Transmission lines with their "to" bus connected to node n.

NL_b^- Transmission lines with their "from" bus connected to node n.
NG_b Generators connected to node n.
NW_b Wind Farms connected to node n.

Variables
C_t^d Dispatch cost of base case at time t.
$C_{t,\phi}^d$ Dispatch cost of distribution ϕ at time t.
P_{gt} Real power generation of generator g at time t.
P_{gt}^{seg} Real power generation of generator g at time t in segment seg.
$P_{wt,s}^W$ Wind generation of wind farm w in scenario s at time t.
P_t^{WC} Total wind curtailment of base case at time t.
$P_{wt,s}^{WC}$ Wind curtailment of wind farm w in scenario s at time t.
$P_{t,\phi}^{WC}$ Total wind curtailment of distribution ϕ at time t.
P_t^{FLC} Total flexible load curtailment of base case at time t.
$P_{bt,s}^{FLC}$ Flexible load curtailment of bus b in scenario s at time t.
$P_{t,\phi}^{FLC}$ Total flexible load curtailment of distribution ϕ at time t.
$PL_{lt,s}$ Real power flow through transmission line l at time t in scenario s.
SR_{gt}^D FR down available through generator g at time t.
SR_{gt}^U FR up available through generator g at time t.
$sr_{gt,s}^D$ FR down deployment by generator g at time t in scenario s.
$sr_{gt,s}^U$ FR up deployment by generator g at time t in scenario s.
$\theta_{1t,s}$ Voltage angle at the slack bus at time t in scenario s.
$\mu_{t,\phi}^{UNC}$ Uncertainty price of distribution ϕ at time t.

Parameters
G Total number of generators.
P_{bt}^D Load at bus b at time t.
P_{rate} Rated output of the wind farm.
PL_l^{max} Upper real power flow limit of transmission line l.
N Number of piece-wise linear segments for the generators.
P_g^{max} Upper generation limit of generator g.
P_g^{min} Lower generation limit of generator g.
RD_g Per minute ramp-down rate for generator g.
RU_g Per minute ramp-up rate for generator g.
S Total number of scenarios.
T Length of investigated time period.
$P_g^{seg,max}$ Upper generation limit of generator g in segment seg.
μ_g^{seg} Linear cost of generator g in segment seg.
μ_g^{sr} FR deployment cost of generator g.
μ_g^{SR} FR capacity cost of generator g.
μ_w^{WC} Wind curtailment compensation rate for wind farm *w.*
μ_b^{FLC} Flexible load curtailment compensation rate for bus b.

v Wind speed.
$f(v)$ The frequency rate of wind speed.
v_{ci} The cut-in speed of the wind turbine.
v_{co} The cut-out speed of the wind turbine.
v_{rated} The rated speed of the wind turbine.
μ Mean value.
σ Standard deviation.
k Shape parameter of Weibull/Rayleigh distribution.
c Scale parameter of Weibull/Rayleigh distribution.
α Shape parameter of Gamma distribution.
β Scale parameter of Gamma distribution.
Γ The Gamma function.
$\gamma_{t,s}$ Probability of scenario s at time t.

2.2 INTRODUCTION

Currently, electric power generation contributes more than 30% of greenhouse emissions in the U.S. It is expected that the electricity demand will grow by 56% from 2010 to 2040 [1], raising an extended concern of the environmental impact caused by power systems. To reduce greenhouse gas emissions, the usage of renewable energy systems (RES) plays a critical role. Among different categories of RES, wind energy has been leading in both the growth and total consumption. In 2017, 52% of global renewable energy consumption is from wind energy, while only 21% is from solar energy. The massive increase in wind energy usage compared to other RES is mainly due to its wide availability and low cost. Wind farms can be deployed not only on land, but also onshore and offshore with large capacities, thus alleviating the need for large areas of land. From 2008 to 2015, wind energy reduced electric power generation cost by one-third [2]. However, the wide usage of RES, such as wind energy, caused a challenge to power system operations due to its risks, which can compromise their economic benefits and negatively affect the reliability of the system if not addressed properly. The risks of renewable energy mainly include two aspects: variability and uncertainty. The variability of renewable energy is relatively easy to accommodate because dispatchable energy resources could be properly scheduled to

accommodate the fluctuation of renewable energy supply if the fluctuations can be accurately forecasted. To accommodate the uncertainty of renewable energy, however, is a true challenge. To mitigate the impact of the uncertainty, renewable energy output forecasting is the first step. Forecasting methods have evolved during the past years, with the goal of reducing error and improving accuracy. The first type of methods are physical methods, which utilize mainly physical data to produce a weather and wind forecast over a period of time [3]. A more sophisticated version of physical methods includes the usage of spatial correlation models, which use the spatial relationship of different wind sites speed data and physical properties. The data obtained from specific sites is used to predict the wind speed at such sites by analyzing the patterns and important parameters of such data [4], [5]. To analyze the data, statistical methods are commonly used. These methods are based on probability density functions (PDF), which provide a good model to portray the pattern of future wind speed and wind power output. Wind power output scenarios can be created through Monte Carlo simulations based on the PDFs, allowing power system operators to take the uncertainty into consideration [6]. The advantage of the statistical methods is their easiness to implement, however, they have relatively large prediction errors as the forecasted time increases [7]. Facilitated by the recent development in artificial intelligence (AI), modern techniques take full advantage of the computational power to perform forecasting tasks. AI algorithms such as artificial neural networks (ANN) are capable of detecting complex nonlinear relations utilizing historical data to determine the dependance between different variables affecting the wind speed forecast with a high accuracy level [8]. Despite the improvement of renewable energy output forecasting methods, forecasting errors are unavoidable. Such forecasting errors are a major source of uncertainty for renewable energy. One of the most prevailing methods to address such uncertainty is to use fast response flexible ramp (FR) [9]. FR, or “flexiramp”, which allows the

generators to rapidly reduce their generation when wind power supply increases and increase their generation when wind power supply decreases based on the fast-ramping capabilities of such generators. It provides the flexibility needed by power system to accommodate the uncertainties of renewable energy resources [10]-[12]. California Independent System Operator (CAISO) and Midcontinent Independent System Operator (MISO) have both adopted FR to manage the variability and uncertainty caused by renewable energy in their systems [13]. The scheduling of FR can be performed using stochastic programming [10], which considers different realizations of the uncertainty, or robust programming [14], which considers the worst-case scenario of the uncertainty. To include FR in the operating schedule can induce an increase in the power system operating cost, which is an opportunity cost that could have been avoided had the FR not been scheduled. In the electricity market, this opportunity cost is often used to determine the price of ancillary services such as FR [14]-[16]. With the procurement of FR due to the integration of renewable energy, the operating costs of the power system will increase inevitably. The impact of wind power uncertainty on the electricity market has been discussed in multiple studies. The impact of wind power on operating reserves is analyzed from a unit commitment and market point of view in [17] and [18]. In the case of [19], the impact of wind power uncertainty on electricity prices were examined. FR products are used to mitigate the impact of wind power uncertainty in [10]-[16], [20]-[23], using either robust optimization [14], [20], which considers the worst-case scenario, or stochastic optimization [10], [11], [21]-[23], which considers a number of uncertainty scenarios. Despite existing studies on the scheduling of ancillary services considering the uncertainty of wind power, there is still a gap in studying the impact of wind power uncertainty on the increase of power system operating costs, and there lacks a comprehensive approach that evaluates the prices of wind power uncertainty with a high time resolution and a large number of

representative scenarios. To address such gaps, this chapter proposes an approach to evaluate the impact of wind power uncertainty on the scheduling of FR products in a stochastic optimization framework and proposes a method to price the uncertainty of wind power. The contributions of this chapter of the thesis are listed as follows:

1. A method to price wind power uncertainty is proposed. The wind power uncertainty prices generated from this method can provide references for electricity market operators to design new market mechanisms and incentivize wind energy builders to mitigate the impact of such uncertainties.
2. A method to evaluate the impact of wind power uncertainty on the scheduling of FR products in proposed in a stochastic optimization framework. This framework avoids producing overly conservative results for scheduling FR products while ensuring that the FR scheduling is representative to show the impact of wind power uncertainty.
3. The method was implemented on a modified RTS-96 test system with high penetration of wind energy and 200 wind power scenarios from three different PDFs were considered. The impact of wind uncertainty represented by different distributions were compared, and the uncertainty of wind power is priced.

The rest of the chapter is organized as follows. Section 2.3 presents wind power uncertainty pricing model, and Section 2.4 specifies the parameters used for the case studies. Simulation results and discussion is presented in section 2.5, followed by the conclusions in section 3.6.

2.3 THE UNCERTAINTY PRICE MODEL

The proposed uncertainty pricing model includes two steps. The first step is to optimally schedule FR in the system using a scenario-based stochastic optimization model. Using this model, the generation dispatch costs for two cases are obtained: (1) the case considering wind power

uncertainty, and (2) the case that assumes wind power is accurately forecasted without uncertainty. In the second step, the difference between the generation dispatch costs obtained in the two cases are calculated, and an average cost increase induced by the uncertainty for each megawatt of wind power is calculated, and this average cost increase per megawatt is considered as the uncertainty price for wind power. The evaluation process is shown in Fig. 2.1.

2.3.1 The Optimal FR Scheduling Model

The optimal FR scheduling model is based on a multi-period stochastic generation dispatch model with 5-minute intervals. This model considers a large number of renewable power generation scenarios and tries to accommodate different scenarios using FR. The curtailment of renewable energy and flexible load is allowed but penalized with high prices in the objective function. The formulation of the model is presented with Equations (2.1)-(2.16). The model objective function shown in (2.1) is to minimize the dispatch cost by considering piecewise linear generation cost, FR capacity cost, and FR deployment cost, as well as wind energy curtailment and flexible load curtailment. Equations (2.2) and (2.3) are the generation constraints, (2.4) is the power balance constraint at each node of the system, (2.5) sets the transmission line thermal limit constraints, (2.6) and (2.7) are the FR availability constraints for each generator, (2.8) set the limit for flexible load curtailment, (2.9) set the limit for wind power curtailment, (2.10) and (2.11) are the 5-minute ramping constraints for each generator, (2.12) is the flexible ramp up constraint while (2.13) corresponds to the flexible ramp down constraint, (2.14) and (2.15) are the flexible ramp up and down deployment constraints, and (2.16) sets Bus 1 as the reference bus.

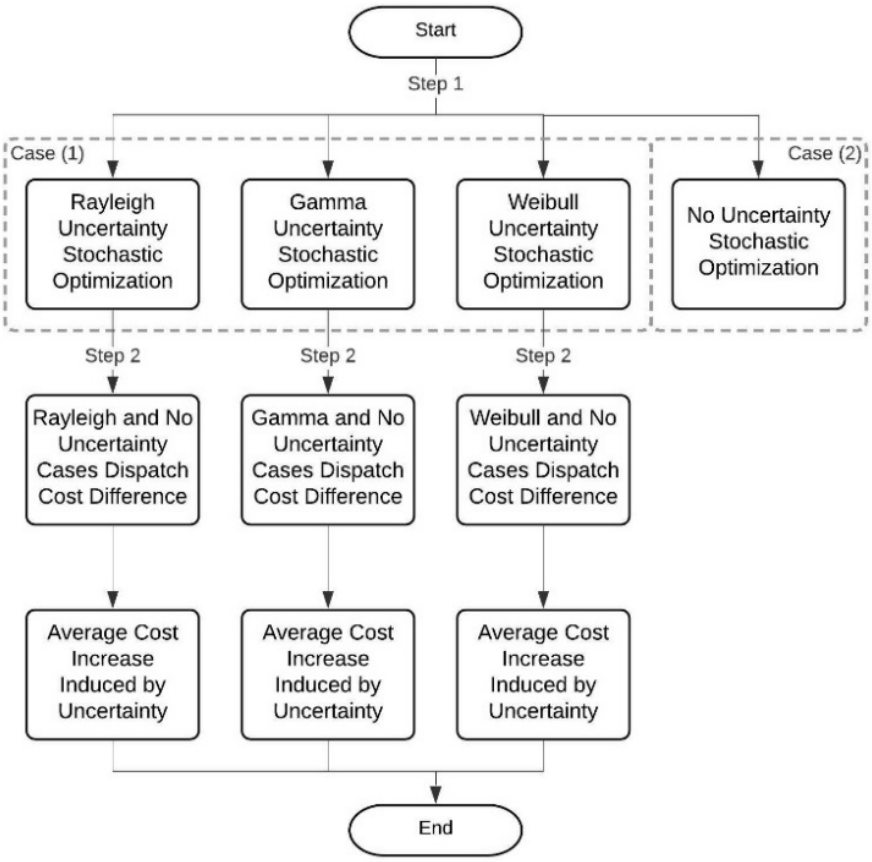

Figure 2.1: Uncertainty Price Model Flowchart

Objective:

$$min\left\{\sum_{t=1}^{T}\sum_{g=1}^{G}\left(\mu_g^{SR}SR_{gt}^{U}+\mu_g^{SR}SR_{gt}^{D}+\sum_{seg=1}^{N}\mu_g^{seg}P_{gt}^{seg}\right)\right.$$
$$+\sum_{t=1}^{T}\sum_{g=1}^{G}\sum_{s=1}^{S}\gamma_{t,s}\left(\mu_g^{sr}sr_{gt,s}^{U}+\mu_g^{sr}sr_{gt,s}^{D}\right)$$
$$+\sum_{=1}^{T}\sum_{b=1}^{B}\sum_{s=1}^{S}\gamma_{t,s}\left(\mu_b^{FLC}P_{bt,s}^{FLC}\right)$$
$$\left.+\sum_{t=1}^{T}\sum_{w=1}^{W}\sum_{s=1}^{S}\gamma_{t,s}\mu_w^{WC}P_{wt,s}^{WC}\right\} \quad (2.1)$$

Constraints:

$$P_{gt}=\sum_{seg=1}^{N}P_{gt}^{seg} \qquad \forall g,t \ (2.2)$$

$$0\le P_{gt}^{seg}\le P_{gt}^{seg,max} \qquad \forall g,t,seg \ (2.3)$$

$$\sum_{i\in NG_b}(P_{gt}^{seg}+sr_{gt,s}^{U}-sr_{gt,s}^{D})+\sum_{w\in NW_b}(P_{wt,s}^{W}-P_{wt,s}^{WC})+\sum_{l\in NL_b^{+}}PL_{lt,s}-\sum_{l\in NL_b^{-}}PL_{lt,s}=P_{bt}^{D}-P_{bt,s}^{FLC} \quad \forall b,t,s \ (2.4)$$

$$-PL_l^{max}\le P_{lt,s}\le PL_l^{max} \quad \forall l,t,s \ (2.5)$$

$$SR_{gt}^{U}+P_{gt}\le P_g^{max}I_{gt} \quad \forall g,t\ge 2 \ (2.6)$$

$$P_g^{min}I_{gt}\le -SR_{gt}^{D}+P_{gt} \quad \forall g,t\ge 2 \ (2.7)$$

$$0\le P_{bt,s}^{FLC}\le P_{bt}^{D} \quad \forall g,t \ (2.8)$$

$$0\le P_{wt,s}^{WC}\le P_{wt,s}^{W} \quad \forall w,t,s \ (2.9)$$

$$P_{gt}-P_{g(t-1)}\le 5RU_g \quad \forall g,t,s\ge 2 \ (2.10)$$

$$P_{g(t-1)}-P_{gt}\le 5RD_g \quad \forall g,t,s\ge 2 \ (2.11)$$

$$0\le SR_{gt}^{U}\le 5RU_g \quad \forall g,t \ (2.12)$$

$$0\le SR_{gt}^{D}\le 5RD_g \quad \forall g,t \ (2.13)$$

$$0\le sr_{gt,s}^{U}\le SR_{gt}^{U} \quad \forall g,t,s \ (2.14)$$

$$0\le sr_{gt,s}^{D}\le SR_{gt}^{D} \quad \forall g,t,s \ (2.15)$$

$$\theta_{1,t,s}=0 \quad \forall g,t,s \ (2.16)$$

2.3.2 The Wind Power Generation Uncertainty Model

In the stochastic FR scheduling model, the uncertainty is modeled through renewable power generation scenarios. In this study, we use wind power as an example. In order to generate the scenarios, first, the mean and standard deviation of the wind speed for each time interval is calculated based on historical wind data. Historical wind data can be obtained through different sources, and one of them is the NREL Wind Prospector [24]. Then, a desired number of wind speed scenarios can be generated through commonly used wind speed distributions, such as Gamma, Weibull, and Rayleigh. At last, wind power generation are calculated based the wind speed in each time interval in each scenario. Different spatiotemporal characteristics need to be considered when selecting an appropriate PDF that properly models the region wind speed characteristics. The most commonly used PDF in wind speed modeling is the Weibull distribution

[25] – [29]. It has been used in the estimation of some wind power generation systems [30] and wind turbines failure analysis [31]. Nevertheless, Weibull is not suitable for locations with very low or very high wind speed [28]. Meanwhile, the Gamma distribution, another widely used distribution to model wind speed [32], is suitable for very low or very high wind speeds, and regions with different underlying surfaces and climatic conditions [28]. The Rayleigh distribution is a special form of the Weibull distribution. Because it is easy to estimate the parameters of the Rayleigh distribution [28], it is also commonly used to model wind speed and evaluate the performance of wind turbines [33], [34].

The Gamma distribution is shown in Equation (2.17), followed by the respective Gamma shape and scale parameters, which are calculated by Equations (2.18) and (2.19), respectively [35].

$$f(v) = \frac{v^{\alpha-1}}{\beta^{\alpha}\Gamma(\alpha)}\ exp\ (-\frac{v}{\beta}) \tag{2.17}$$

$$\beta = \frac{\sigma^2}{\mu} \tag{2.18}$$

$$a = \frac{\mu^2}{\sigma^2} \tag{2.19}$$

The Weibull distribution is presented in (2.20). Similar to the Gamma distribution, the shape parameter and scale parameter are calculated using the mean and standard deviation of the wind speed in Equations (2.21) and (2.22), respectively. One of the main limitations of the Weibull probability density function (PDF), as criticized by [36], is the lack of accuracy when representing probabilities of observing low wind speed values or zero wind cases.

$$f(v) = \frac{k}{c}\left(\frac{v}{c}\right)^{k-1} exp\left(-\left(\frac{v}{c}\right)\right)^{k} \tag{2.20}$$

$$k = \left(\frac{\sigma}{\mu}\right)^{-1.086} \tag{2.21}$$

$$c = \frac{\mu}{\Gamma(1+k^{-1})} \tag{2.22}$$

Lastly, the Rayleigh distribution is a special formulation of the Weibull distribution, following the same PDF as (2.20). Rayleigh distribution has a constant scale parameter of k = 2, with the only variable parameter being the shape parameter, as Equation (2.23) shows. Rayleigh distribution has been widely implemented due to its easy implementation by being a single parameter PDF [36].

$$c = \frac{2}{\sqrt{\pi}}\mu \tag{2.23}$$

To calculate the wind power generation according to wind speed, Equation (2.24) is used [37]. The wind power generation model considers three important values: the cut-in speed, a wind speed below which would results in a zero-power output from the wind power generator, the cut-out speed, a wind speed above which would results in a zero-power output from the wind power generator, and the rated wind speed of the turbine. When the wind speed is between the rated speed and cut-out speed, the wind power generator produces a rated amount of power.

$$P_{r,s} = \begin{cases} P_{rate} & if\ v_{rate} \le v \le v_{co} \\ P_{rate}\dfrac{v^3 - v_{ci}^3}{v_{rate}^3 - v_{ci}^3} & if\ v_{ci} \le v \le v_{rate} \\ 0 & otherwise \end{cases} \tag{2.24}$$

2.3.3 The Wind Power Uncertainty Price Calculation

At many locations, the wind speed follows a day and night pattern. Take Texas as an example, the seasonal pattern for the wind speed is not obvious, but the day and night pattern is obvious, since the wind speed is usually higher at night than during the day. To accommodate a 5-minute resolution for the optimal FR scheduling model, the mean and standard deviation of the wind speed for each 5-minute interval is calculated using historical data, and the mean value of the wind speed in each interval is used as the wind speed without uncertainty, and the wind power generation without uncertainty can be calculated accordingly. Then a desired number of wind speed scenarios are generated using the distributions described in Section II-B, and then the wind power generation in each scenario can be calculated.

After the wind power generation without uncertainty and the scenarios with uncertainty are obtained, two cases of optimal FR scheduling can be implemented using the model presented in Section II-A: (1) FR scheduling with only one scenario, the scenario without uncertainty, and (2) FR scheduling with a number of wind power generation scenarios. Then the generation dispatch cost in the two cases can be obtained from part of their objective values:

$$C_{dispatch} = \sum_{seg=1}^{N} \mu_g^{seg} P_{gt}^{seg} \tag{2.25}$$

Then, the uncertainty price can be calculated as:

$$C_{uncertainty} = \frac{C_{dispatch}^{Case\,(2)} - C_{dispatch}^{Case\,(1)}}{P_{average}^{W}} \tag{2.26}$$

2.4 Model Setup and Specifications

2.4.1 Test System

The simulations were performed on a modified RTS-96 test system shown in figure 2.2, and with minor modifications similar to [38]. In this study, the original peak load values of the system were used. The system includes two 200-MW wind farms at bus 3 and 24, respectively.

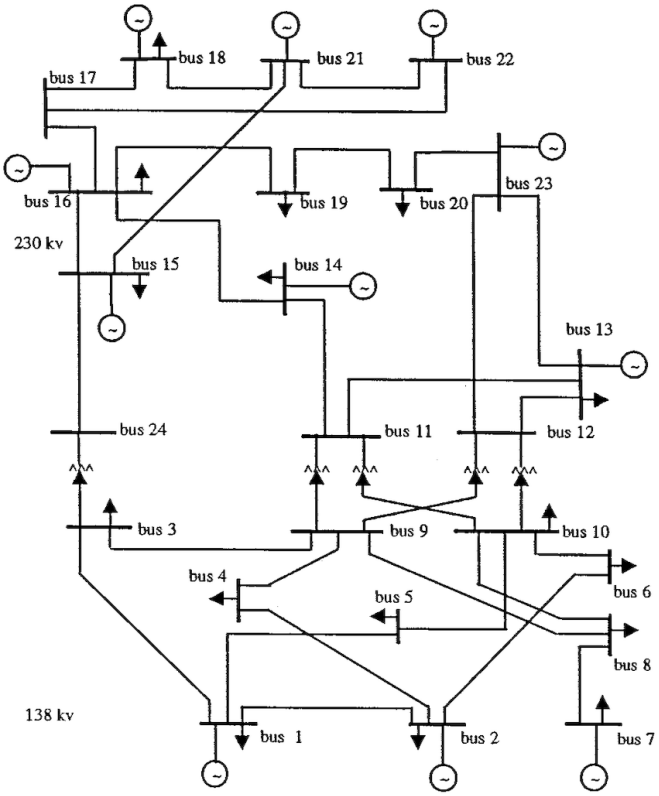

Figure 2.2: RTS-96 Test System [39]

2.4.2 Wind Speed Scenarios

To study the impact of wind power uncertainty, 200 wind speed scenarios on a five-minute resolution were created for the duration of a day using the three wind speed distribution models, Gamma, Rayleigh, and Weibull, as described in Section II-B. To generate these scenarios, the wind speed data of Taylor, TX for the year 2012 were obtained [24], [27], [28], and the mean and standard deviation of the wind speed at each five-minute time point in the January were computed. The mean and standard deviation of the wind speed at each time point were used to create 288 shape parameters c and scale parameters p (i.e., twelve 5-minute intervals each hour for 24 hours) that yielded 288 different PDFs. Using these PDFs, 200 random wind speed values were generated at each time point using the gamrnd, wblrnd, raylrnd functions for Gamma, Weibull, and Rayleigh

PDFs, respectively, in MATLAB (version 2020a). The 200 scenarios allowed the optimization problem to cover a representative amount of uncertainties of the wind speed.

2.4.3 Wind Power Generation for Each Scenario

With the wind speed scenarios generated in Section III-B, the wind power output at each wind speed were calculated using Equation (2.24). The cut-in speed used for the model was 4 m/s, and the cut-out speed was 25 m/s. The rated wind speed was 14m/s, and the rated power output of each wind farm is 200MW. Using the 200 wind speed values for each 5-minutes interval, 200 wind power output scenarios were created for every interval of the day for each PDF. .

2.4.4 Conditions for the Case Studies

In this study, case studies were carried out under five conditions:

i. Only one scenario was considered in the stochastic optimal FR scheduling problem, and wind power generation was assumed to be zero at all times in this scenario.
ii. Only one scenario was considered, and the mean wind speed at each time point was used to generate the wind power output scenario.
iii. 200 scenarios generated from the Gamma distribution were considered.
iv. 200 scenarios generated from the Rayleigh distribution were considered.
v. 200 scenarios generated from the Weibull distribution were considered.

In the stochastic optimal FR scheduling model, wind power curtailment and flexible load curtailment were allowed but penalized in the objective function. The penalties for wind power curtailment and flexible load curtailment were $10,000/MW and $15,000/MW, respectively. In Conditions (i) and (ii), FR was not allowed because there was no uncertainty in the two cases. .

2.5 SIMULATION RESULTS

2.5.1 Uncertainty Analysis

To evaluate the impact of wind speed uncertainty, the deviations of wind speed from its average were evaluated. The deviations were calculated using the wind speed of each five-minute interval during the day in Condition (iii)-(v), respectively, minus the wind speed in Condition (ii), and the process was repeated for each of the 200 scenarios, creating a total of 57600 deviation entries for each of the three distributions.

The histograms in Fig. 2.3 - Fig. 2.5 shows the normalized errors of the deviations. The normalization process was realized by diving each individual error by the maximum absolute error of each distribution. In order to evaluate these deviations, four statistical parameters were obtained from the 57600 deviation entries from each distribution and presented in Table 2.1. The four parameters are mean (μ), standard deviation (σ), kurtosis (κ), and skewness (γ). From the results, it can be seen that the Gamma and Rayleigh distributions tend to underestimate the wind speed, while the Weibull distribution tend to overestimate wind speed, and the standard deviations indicate that the deviations from the Gamma and Rayleigh distributions have a smaller spread and higher concentration of mass near the mean than those from the Weibull distribution [40]. The kurtosis values indicate that the distribution of the deviations from the Gamma and Rayleigh distributions tend to have a higher peak and fatter tail than those from the Weibull distribution. The skewness of the deviations from the three distributions shows that those from the Gamma and Rayleigh distributions tend to lean toward the farther left side than those from the Weibull distribution.

Table 2.1: Error Distributions Parameters.

	μ	σ	κ	γ
Gamma	-0.0002	0.1620	3.879	0.7457
Weibull	0.0007	0.2394	2.787	0.1874
Rayleigh	-0.0886	0.1594	3.624	0.7209

2.5.2 FR Capacity Scheduling

To analyze the FR scheduling with uncertainty represented by different distributions, we calculated the averages of scheduled FR for each hour of the day considering the results from simulations carried out using load profiles in the month of January. The averages in MW are presented in Fig. 2.6. The valley at hour 4 corresponds to small deviations from the average values, which could be addressed by using only a relatively small amount of FR. The spike from Hour 11-16 in the FR down curve shows that there was excessive wind energy generated during these hours from both the Gamma and Weibull distributions, which required conventional, dispatchable resources to ramp down to facilitate the integration of wind energy.

2.5.3 FR Deployment

While FR capacity was scheduled to meet the worst-case scenario in Conditions (iii), (iv), and (v), the deployment of FR varies in each scenario. To analyze FR deployment, we calculated the average percentage of FR deployed for each hour in the day considering the 200 scenarios in an overall length of 31 days. The results are shown in Fig. 2.7. Since FR deployment was co-optimized with generation dispatch, the deployment of FR is determined by a number of factors, such as the availability of wind energy, load profile, and generation dispatch. During night hours, with a low load level and high wind speed, downward FR was more frequently used than upward FR to address the deviations of wind speed. During the day, with a high load level and low wind speed, upward FR was more frequently used than downward FR to address the deviations of the wind speed.

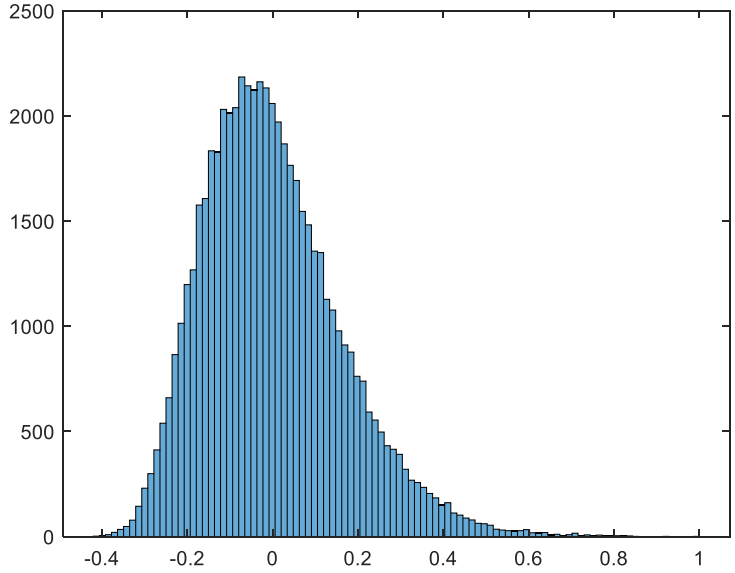

Figure 2.3: Normalized histogram of forecasted Gamma errors

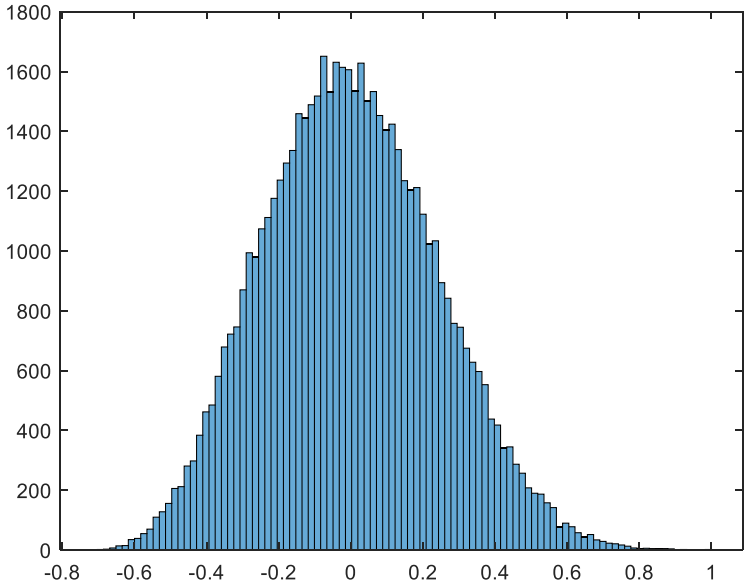

Figure 2.4: Normalized histogram of forecasted Weibull errors

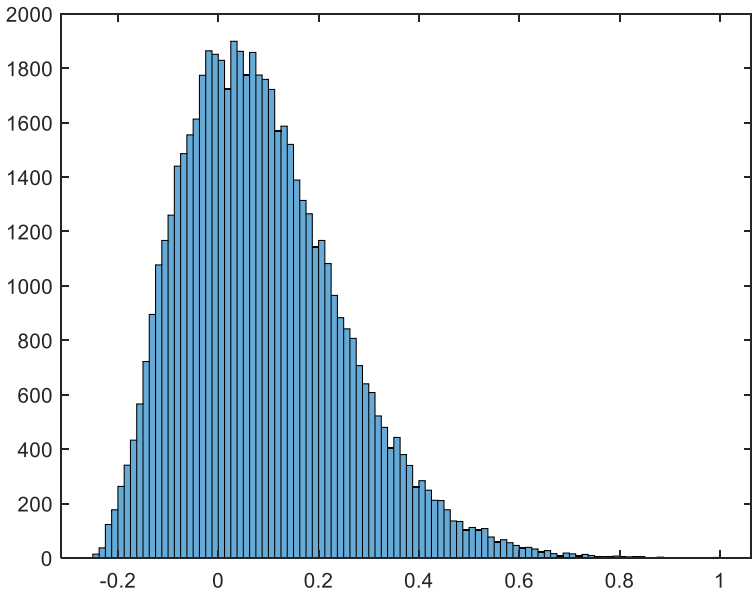

Figure 2.5: Normalized histogram of forecasted Rayleigh errors

2.5.4 Dispatch Cost

Since producing wind energy does not incur a fuel cost, integrating wind energy in a power system can reduce its generation dispatch cost. Fig. 2.8 shows that regardless of uncertainty being present or not, the generation dispatch cost in the case with RES is lower than that without RES. By excluding the cost of FR capacity and FR deployment, the dispatch cost is slightly higher overall in the cases with uncertainty. The difference of dispatch cost in the cases with and without uncertainty are calculated as a percentage of the dispatch cost without uncertainty and shown in Fig. 2.9. Positive percentages indicate that the cases with uncertainties have a higher generation cost than the case without uncertainty. As the figure shows, the average generation dispatch cost is higher in the cases with uncertainty in most hours of the day.

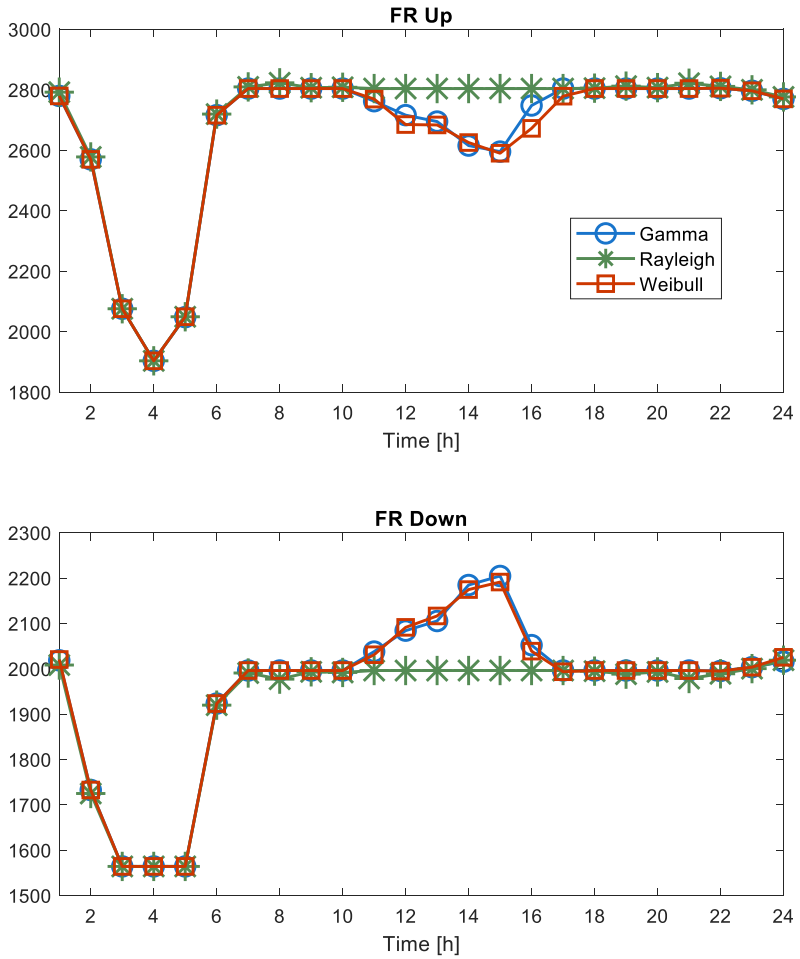

Figure 2.6: Gamma, Weibull, and Rayleigh FR up/down capacity scheduling

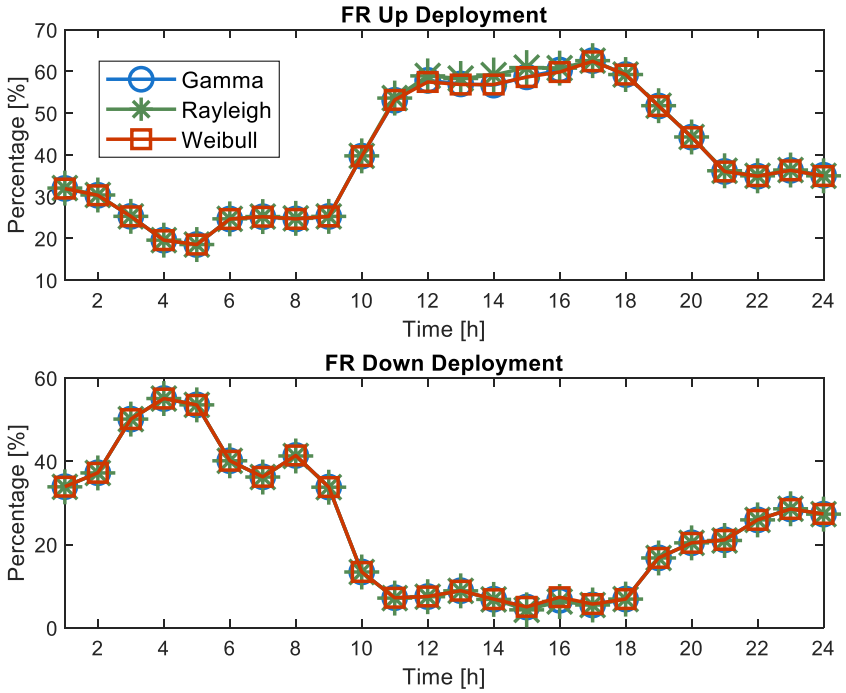

Figure 2.7: Gamma, Weibull, and Rayleigh FR up/down deployment

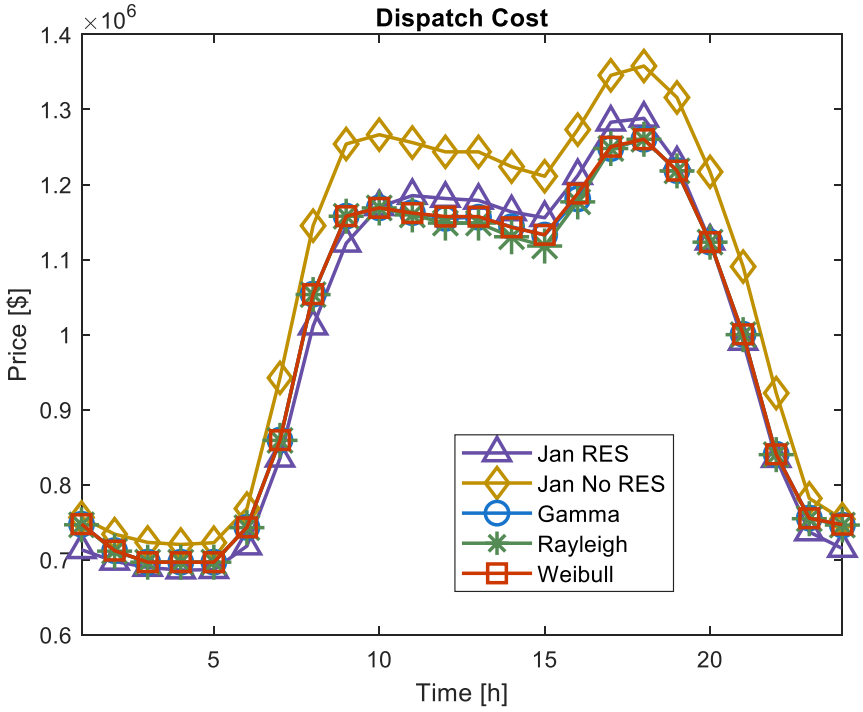

Figure 2.8: Generation Dispatch Cost

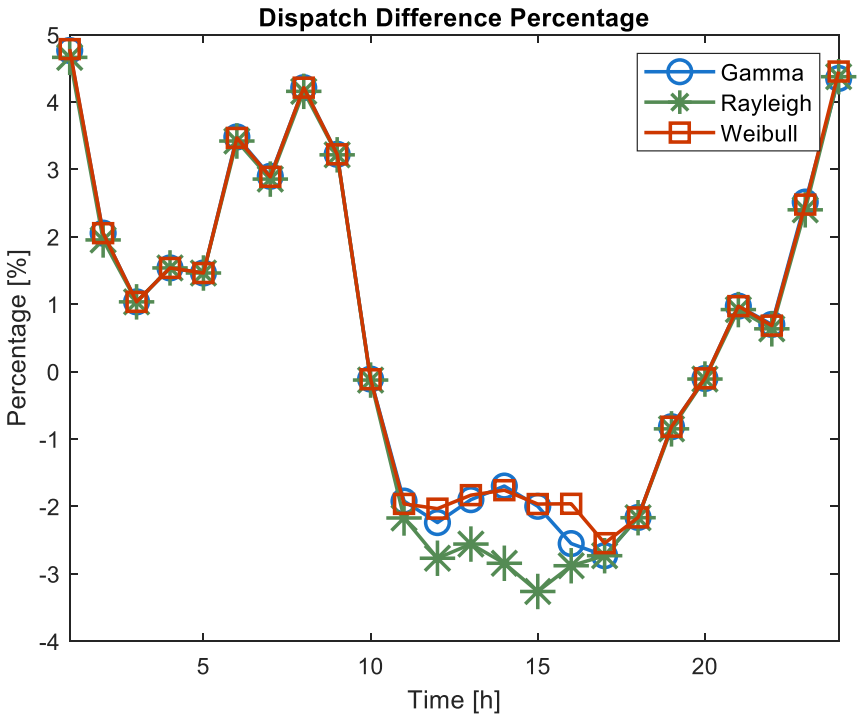

Figure 2.9: Generation dispatch percentage difference

2.5.5 Wind Power Curtailment

The wind power that could not be integrated into the system even with the deployment of FR were curtailed in the model. The average wind power curtailment for each hour of the day is presented in Fig. 2.10. The wind power curtailment in the figure was obtained from the stochastic optimization model with uncertain scenarios generated by Gamma, Rayleigh, and Weibull distributions, respectively. It can be seen from the subplot that wind energy curtailment occurred at night when wind speed was high. For the cases with uncertainty, the case with scenarios from the Rayleigh distribution had the most curtailment among the three cases, this is because Rayleigh distribution tends to underestimate wind speed values, as Table I shows.

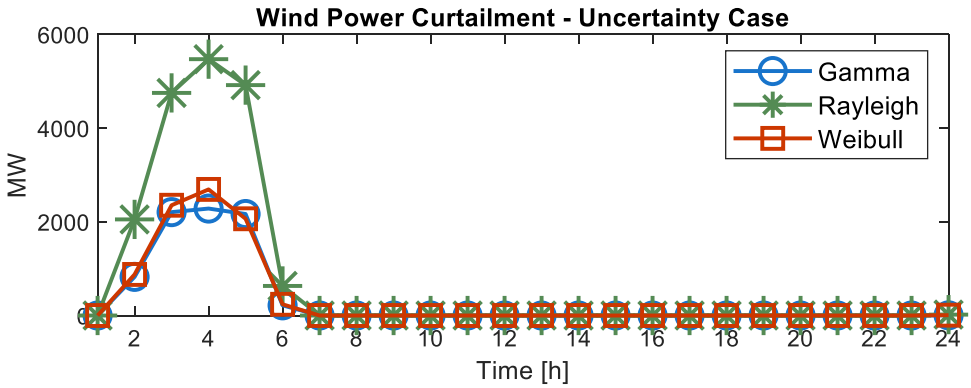

Figure 2.10: Wind power curtailment

2.5.6 Flexible Load Curtailment

Flexible load represents load that could be curtailed during emergencies, such as customers who possess emergency generators and have contract in place with the utility that allows the utility to disconnect them from the grid for a short period of time during emergencies. In the simulations implemented in this study, load curtailment is a very rare condition. The average flexible load curtailment for each hour of the day is presented in Fig. 2.11. As the figure shows, load curtailment only occurred when the Gamma distribution was used to generate the scenarios and the maximum load curtailment was less than 1 MW. The load curtailment was caused by a combination of low actual speed winds and a high expectancy for the availability of wind energy.

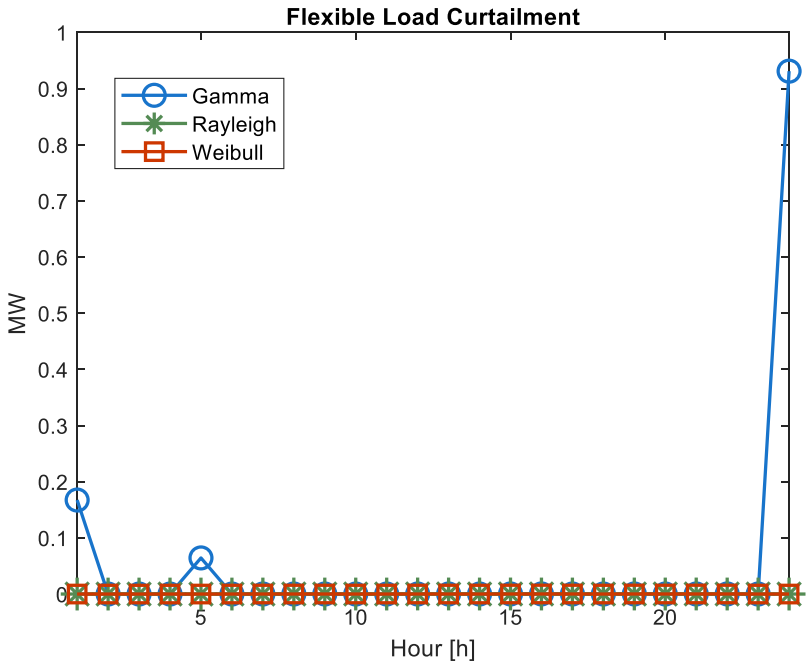

Figure 2.11: Gamma, Weibull, and Rayleigh flexible load curtailment

2.5.7 Uncertainty Price Evaluation

As Section IV-D indicates, uncertainty increases the overall dispatch cost. In this study, uncertainty prices were calculated in Conditions (iii), (iv), and (v). As Equation (2.27) indicates, the uncertainty price is defined as the difference between the total cost in the case with uncertainty and the case without uncertainty. The total cost includes generation dispatch cost, the compensation of wind power curtailment, and penalty of load curtailment. The uncertainty prices of wind power evaluated under each distribution in each hour of the day is shown in Fig. 2.12. In a further uncertainty price comparison, a daily average uncertainty price was computed for each distribution and displayed in Table 2.2. Results show that Rayleigh distribution induced the lowest uncertainty cost, followed by Weibull, and lastly Gamma by presenting the highest uncertainty cost.

$$\mu_{t,\phi}^{UNC} = C_{t,\phi}^{d} + \$\,30/MW\left(P_{t,\phi}^{WC}\right) + \$10000/MW\left(P_{t,\phi}^{FLC}\right) - C_{t}^{d} - \$\,30/MW\left(P_{t}^{WC}\right) - \$10000/MW\left(P_{t}^{FLC}\right) \quad \forall t, \phi \quad (2.27)$$

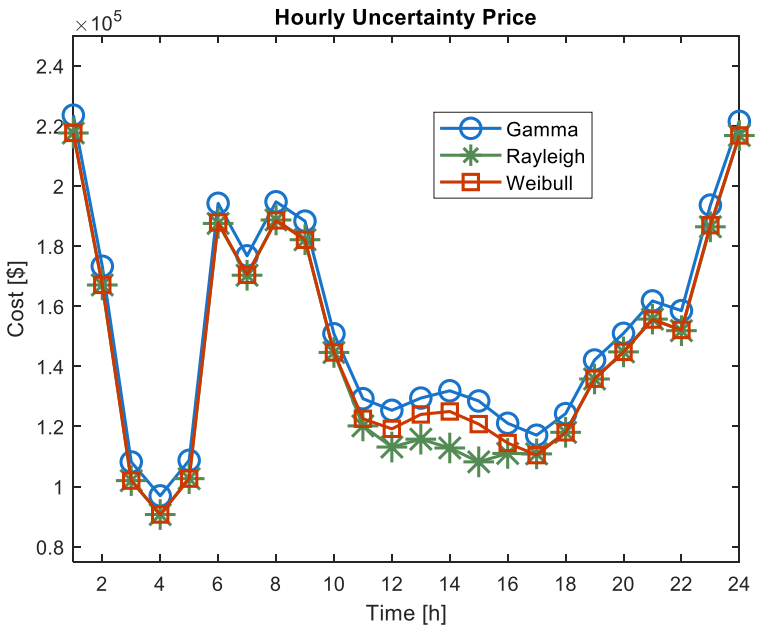

Figure 2.12: Gamma, Weibull, and Rayleigh Hourly Uncertainty Price

Table 2.2: Average Daily Uncertainty Price.

	$/Day
Gamma	152,098.96
Rayleigh	143,927.70
Weibull	145,825.20

2.6 CONCLUSION

This chapter proposes a method to evaluate the uncertainty price of wind power based on a stochastic optimization model. The model was implemented wind speed scenarios generated from the Gamma, Weibull, and Rayleigh distributions. Results show that the model can schedule FR products to effectively address the uncertainty of wind power. The results also show that the uncertainty of wind power increases the generation dispatch cost, wind power curtailment, and load curtailment. Thus, the price of wind power uncertainty can be defined as the sum of the increase in generation dispatch cost, the compensation for wind power curtailment, and penalty of load curtailment. The uncertainty prices differ according to the probability distribution function

used to represent the uncertainty and selecting the right method to represent the uncertainty is important. The method proposed in this study can be used to provide guidance for policy makers and electricity market designers to incentivize the builders to reduce the uncertainty from RES.

2.7 REFERENCES

[1] Y. Kumar, "Wind energy: Trends and enabling technologies," Renewable and Sustainable Energy Reviews, vol. 53, pp. 209-224, 2016.

[2] P. Sadorky, "Wind energy for sustainable development: Driving factors and future outlook," Journal of Cleaner Production, vol. 289, p. 125779, 2021.

[3] X. Zhao, C. Wang, J. Su, and J. Wang, "Research and application based on the swarm intelligence algorithm and artificial intelligence for wind farm decision system," Renewable energy, vol. 134, pp. 681-697, 2019.

[4] A. Lenzi, I. Steinsland, and P. Pinson, “Benefits of spatiotemporal modeling for short-term wind power forecasting at both individual and aggregated levels,” Envirometrics, vol. 29, no. 3, p. e2493, 2018.

[5] Y. Liu, H. Quin, Z. Zhang, S. Pei, Z. Jiang, Z. Feng, and J, Zhou, “Probabilistic spatiotemporal wind speed forecasting based on a variational Bayesian deep learning model,” Applied Energy, vol 260, p. 114259, 2020.

[6] G. Marmidis, S. Lazarou, and E. Pyrgioti, “Optimal placement of wind turbines in a wind park using Monte Carlo simulation,” Renewable Energy, vol. 33, no. 7, pp. 1455-1460, 2008.

[7] W.Y. Chang, “A literature review of wind forecasting methods,” Journal of Power and Energy Enegineering, vol. 2, no. 04, pp. 161, 2014.

[8] H. H. Çevik, M. Çunkaş, and K. Polat, “A new multistage short-term wind power forecast model using decomposition and artificial intelligence methods,” Physica A: Statistical Mechanics and its Applications, vol. 534, p. 122177, 2019.

[9] M. M. Aly, M. Abdel-Akher, S. Said, and T. Senjyu, "A developed control strategy for mitigating wind power generation transients using superconducting magnetic energy storage with reactive power support," Journal of Electrical Power & Energy Systems, vol. 83, pp. 485-494, 2016.

[10] E. Heydarian-Forushani, M.E. Golshan, M. Shafie-khan, and P. Siano, "Optimal operation of emerging flexible resources considering sub-hourly flexible ramp product," IEEE Transactions on Sustainable Energy, vol. 9, no. 2, pp. 916-929, 2017.

[11] B. Wang, and B. F. Hobbs, "A flexible ramping product: Can it help real-time dispatch markets approach the stochastic dispatch ideal?," Electric Power Systems Research, vol. 109, pp. 128-140, 2014.

[12] Q. Wang and B. M. Hodge, "Enhancing power system operation flexibility with flexible ramping products: A review," IEEE Transactions on Industrial Informatics, vol. 13, no. 4, pp. 1652-1664, 2016.

[13] N. Navid and G. Rosenwald, "Ramp capability product design for MISO markets," Midcontinent Independent System Operator, Carmel, IN, USA, Jul. 10, 2013. [Online]. Available: https://www.misoenergy.org/Library/Repository/Communication%20Material/Key%20Presentations%20and%20Whitepapers/Ramp%20Product%20Conceptual%20Design%20Whitepaper.pdf

[14] H. Ye and Z. Li, "Deliverable Robust Ramping Products in Real-Time Markets," IEEE Trans. Power Syst., vol. 33, no. 1, pp. 5–18, Mar. 2017.

[15] E. Ela, V. Gevorgian, A. Tuohy, B. Kirby, M. Milligan, and M. O'Malley, "Market designs for the primary frequency response ancillary service-Part I: Motivation and design," IEEE Trans. Power Syst., vol. 29, no. 1, pp. 421–431, Jan. 2014.

[16] E. Ela and M. O'Malley, "Scheduling and Pricing for Expected Ramp Capability in Real-Time Power Markets," IEEE Trans. Power Syst., vol. 31, no. 3, pp. 1681–1691, May 2016.

[17] J. Kiviluoma, M. O'Malley, A. Tuohy, P. Meibom, M. Milligan, B. Lange, H. Holttinen, and M. Gibescu, "Impact of wind power on the unit commitment, operating reserves, and market design," IEEE PES General Meeting, pp. 1–8, 2011.

[18] A. Botterud, Z. Zhou, J. Wang, J. Valenzuela, J. Sumaili, R. J. Bessa, H. Keko, and V. Miranda, "Unit commitment and operating reserves with probabilistic wind power forecast," IEEE PowerTech, 2011.

[19] J. Cardell, L. Anderson, and C. Y. Tee, "The effect of wind and demand uncertainty on electricity prices and system performance," IEEE PES T&D 2010, pp. 1-4, 2010.

[20] X. Fang, K. S. Sedzro, H. Yuan, H. Ye and B.-M. Hodge, "Deliverable Flexible Ramping Products Considering Spatiotemporal Correlation of Wind Generation and Demand Uncertainties," IEEE Trans. Power Syst., vol. 35, no. 4, pp. 2561-2574, July 2020.

[21] G. Zhang and J. McCalley, "Stochastic look-ahead economic dispatch with flexible ramping product," in Proc. 2015 IEEE Power & Energy Society General Meeting, Denver, CO, 2015, pp. 1-5.

[22] M. A. Mirzaei, M. Nazari-Heris, B. Mohammadi-Ivatloo and M. Marzband, "Consideration of Hourly Flexible Ramping Products in Stochastic Day-Ahead Scheduling of Integrated Wind and Storage Systems," in Proc. 2018 Smart Grid Conference (SGC), Sanandaj, Iran, 2018, pp. 1-6.

[23] M. A. Mirzaei et al., "Network-Constrained Joint Energy and Flexible Ramping Reserve Market Clearing of Power- and Heat-Based Energy Systems: A Two-Stage Hybrid IGDT–Stochastic Framework," IEEE Systems Journal, vol. 15, no. 2, pp. 1547-1556, June 2021.

[24] "The Wind Prospector", National Renewable Energy Laboratory [Online]. Available: https://maps.nrel.gov/wind-prospector/

[25] D. Petković, S. Shamshirband, N. B. Anuar, H. Saboohi, A. W. Abdul Wahab, M. Protić, et al, "An Appraisal of Wind Speed Distribution Prediction by Soft Computing Methodologies: A Comparative Study," Energ. Convers. Manag. 84, pp. 133–139, 2014.

[26] P. Wais, "Two and Three-Parameter Weibull Distribution in Available Wind Power Analysis," Renew. Energ. 103, pp. 15–29, 2017.

[27] A. Sarkar, G. Gugliani, and D. Deep, "Weibull Model for Wind Speed Data Analysis of Different Locations in India," KSCE J. Civ Eng. 21 (7), 2017.

[28] S. Huanyu, D. Zhibao, X. Nan, and H. Qinni, 'Wind Speed Distributions Used in Wind Energy Assessment: A Review," Frontiers in Energy Research, pp. 790, 2021.

[29] R. I. Harris, and N. J. Cook, "The Parent Wind Speed Distribution: Why Weibull?," J. Wind Eng. Ind. Aerod 131, pp. 72–87, 2014

[30] A. N. Celik, "A Simplified Model for Estimating Yearly Wind Fraction in Hybrid-Wind Energy Systems. Renew," Energ. 31 (1), pp. 105–118, 2006.

[31] X, Jin, Y. Chen, L. Wang, H. Han, and P. Chen, "Failure Prediction, Monitoring and Diagnosis Methods for Slewing Bearings of Large-Scale Wind Turbine: A Review," Measurement 172, 108855, 2021.

[32] N. Aries, S. M. Boudia, and H. Ounis, "Deep Assessment of Wind Speed Distribution Models: A Case Study of Four Sites in Algeria," Energ. Convers. Manag. pp. 155, 78–90. 2018.

[33] H. Saleh, A. Abou El-Azm Aly, and S. Abdel-Hady, "Assessment of Different Methods Used to Estimate Weibull Distribution Parameters for Wind Speed in Zafarana Wind Farm, Suez Gulf, Egypt," Energy 44 (1), pp. 710–719, 2012.

[34] G. Valencia Ochoa, J. Núñez Alvarez, and M. Vanegas Chamorro, “Data Set on Wind Speed, Wind Direction and Wind Probability Distributions in Puerto Bolivar – Colombia,” Data Brief 27, 104753, 2019.

[35] J. Zhou, E. Erdem, G. Li and J. Shi, "Comprehensive evaluation of wind speed distribution models: A case study for North Dakota sites", Energy Conversion and Management, vol. 51, pp. 1449-1458, 2010.

[36] J. Yingni, Y. Xiuling, C. Xiaojun, and P. Xiaoyun, "Wind potential assessment using the Weibull model at the Inner Mongolia of China," Energy exploration & exploitation, vol. 24, no. 3, pp. 211-221, 2006.

[37] Y. Sang and Y. Zheng, "Reserve Scheduling in the Congested Transmission Network Considering Wind Energy Forecast Errors," IEEE Transactions on Energy Conversion, vol. 23, pp. 592-602, 2008.

[38] Y. Sang, M. Sahraei-Ardakani, and M. Parvania, "Stochastic transmission impedance control for enhanced wind energy integration," IEEE Transactions on Sustainable Energy, vol. 9, no. 3, pp. 1108-1117, 2017.

[39] C. Grigg et al., "The IEEE Reliability Test System-1996. A report prepared by the Reliability Test System Task Force of the Application of Probability Methods Subcommittee," in IEEE Transactions on Power Systems, vol. 14, no. 3, pp. 1010-1020, Aug. 1999

[40] H. Bludszuweit, J. A. Domínguez-Navarro, and A. Llombart, "Statistical analysis of wind power forecast error," IEEE Transactions on Power Systems, vol. 23, pp. 983-991, 2008.

Chapter 3: Computational Challenges in the big-M OTS Problem

As more RESs are integrated into the power system better congestion management strategies are required to maintain power reliability. One of the solutions to reduce transmission system congestion is to increase grid flexibility and implementing flexible topology control by allowing OTS. This chapter includes a published paper that highlights the computational challenges of big-M OTS decision-making problems. [1]

Transmission switching is widely used in the electric power industry for both preventive and corrective purposes. Optimal transmission switching (OTS) problems are usually formulated based on optimal power flow (OPF) problems. OTS problems are originally nonlinear optimization problems with binary integer variables indicating whether a transmission line is in or out of service, however, they can be linearized into mixed-integer linear programs (MILP) through the big-M method. In such big-M-based MILP problems, the value of M can significantly affect their computational efficiency. This chapter proposes a method to find the optimal big-M values for OTS problems and studies the impact of big-M values on the computational efficiency of OTS problems. The model was implemented on a modified RTS-96 test system, and the results show that the proposed model can effectively reduce the computational time by finding an optimal big-M value which ensures optimal switching solutions while maintaining numerical stability.

3.1 NOMENCLATURE

Indices

b	Bus.
g	Generator.
k	Transmission Line.
s	Scenario.
seg	Segments for piece-wise linear cost function.
t	Time.

Sets

σ_b^+	Transmission lines with their "to" bus connected to bus b.
σ_b^-	Transmission lines with their "from" bus connected to bus b.

[1] Reprinted with permission from L. Ramirez-Burgueno, Y. Sang, and N. Santiago, "Improving the Computational Efficiency of Optimal Transmission Switching Problems," *IEEE*

g_b Generators connected to bus b.

Variables

$\theta_{b,t,s}$ Voltage angle of bus b at time t in scenario s.

$\theta_{fr,k,t,s}$ Voltage angle at the "from" bus of line k at time t in scenario s.

$\theta_{to,k,t,s}$ Voltage angle at the "to" bus of line k at time t in scenario s.

M_t Big-M value at time t.

$P_{g,t}$ Real power generation of generator g at time t.

$P_{g,t}^{seg}$ Real power generation of generator g at time t in segment seg.

$P_{b,t,s}^{W}$ Wind generation of wind farm at bus b at time t in scenario s.

$P_{b,t,s}^{WC}$ Wind curtailment of wind farm at bus b at time t in scenario s.

$P_{b,t,s}^{LC}$ Flexible load curtailment of bus b at time t in scenario s.

$F_{k,t,s}$ Real power flow through transmission line k at time t in scenario s.

$SR_{g,t}^{D}$ Spinning down reserve available through generator g at time t.

$SR_{g,t}^{U}$ Spinning up reserve available through generator g at time t.

$sr_{g,t,s}^{D}$ Spinning down reserve deployed by generator g at time t in scenario s.

$sr_{g,t,s}^{U}$ Spinning up reserve deployed by generator g at time t in scenario s.

$Z_{k,t}$ Transmission switching binary status (1: line k is on at time t; 0: line k is off at time t).

Parameters

$\gamma_{t,s}$ Probability of scenario s at time t.

θ_k^{min} Minimum voltage angle difference at line k.

θ_k^{max} Maximum voltage angle difference at line k.

$\theta_{1,t,s}$ Voltage angle at the slack bus at time t in scenario s.

B Total number of buses.

b_k Susceptance of transmission line k.

G Total number of generators.

M_{max} The maximum value of the big M.

$P_{b,t}^{L}$ Load at bus b at time t.

F_k^{max} Upper real power flow limit of transmission line l.

N Number of piece-wise linear segments for the generators.

P_g^{max} Upper generation limit of generator g.

P_g^{min} Lower generation limit of generator g.

P_{rate} Rated output of the wind farm.

$P_g^{seg,max}$ Upper generation limit of generator g in segment seg.

R_g Per minute ramp rate for generator g.

S Total number of scenarios.

T Length of investigated time period.

$u_{g,t}$ Generator binary status (1: generator g is on at time t; 0: generator g is off at time t.

$u_{g,t}^{SD}$ Shutdown binary indicator (1: generator g shuts down at time t; 0: generator g does not shut down at time t).

$u_{g,t}^{SU}$ Startup binary indicator (1: generator g starts up at time t; 0: generator g does not start up at time t).

Z_k^F Transmission line failure at line k.

Z_k^{max} Maximum lines permitted for transmission switching.

μ_g^{seg} Linear cost of generator g in segment seg.

μ^M M penalty cost.

μ_g^{NL} No load cost of generator g.

μ_g^{sr} Spinning reserve deployment cost of generator g.

μ_g^{SR} Spinning reserve capacity cost of generator g.

μ_g^{SD} Shutdown cost of generator g.

μ_g^{SU} Startup cost of generator g.

μ^{WC} Wind curtailment compensation rate.

μ_b^{FLC} Flexible load curtailment compensation rate for bus b.

v Wind speed.

$f(v)$ The frequency rate of wind speed.

v_{ci} The cut-in speed of the wind turbine.

v_{co} The cut-out speed of the wind turbine.

v_{rated} The rated speed of the wind turbine.

3.2 INTRODUCTION

The rising environmental awareness has boosted the usage of RESs, which plays a crucial role in reducing the usage of fossil fuel-based electric power as well as providing economic benefits to the users. However, RESs introduces significant uncertainty to power systems, resulting in power system stability and reliability concerns, and various techniques are currently being used to improve system flexibility for increased RES penetration to improve the reliability and cost efficiency of power systems [1]-[3]. Among different techniques, appropriately adjusting the network topology of electric power transmission systems through optimal transmission switching (OTS) can result in great benefits such as reduced transmission congestion, improved voltage profiles, better system security, and reduced operating costs [4]-[8].

Currently, OTS problems are usually formulated based on optimal power flow (OPF) problems by modifying the power flow constraints with the introduction of binary integer variables that indicate whether the transmission line is in or out of service. The OTS problem is originally a nonlinear optimization problem, and the big-M method is usually used to linearize the problem, making the problem a mixed-integer linear program (MILP). Although the linearization helps improve the computational efficiency of the OTS problem, the MILP is still relatively computation, especially for large-scale, real-world power systems [9]. Thus, improving the computational efficiency of the OTS problem is paramount.

In the big-M method, binary variables are used to enable or disable constrains, leading to big-M constraints in the form of (3.1), where x represents a binary variable and M corresponds to a "big constant" [10]:

$$a'y + M(1 - x) \geq b \tag{3.1}$$

The selection of M has a significant impact on the computational efficiency of MILP problems. A poorly selected M value can lead to non-optimal solutions or an unnecessarily long solution time [11], [13]. It is common in literature and research to advocate selecting a very large number as the value of M, however, an unnecessarily large value of M can expand the feasible region of the MILP problem, resulting in an increased number of iterations required to obtain the optimal solution [11], [12] and thus negatively affect the computational efficiency of the problem. Furthermore, an extremely large value of M can even cause a loss of solver's precision and numerical instability [13], [14]. In additional to the previously mentioned scenarios, a small M value limits the feasible region space. Consequently, a small M does not guarantee the convergence to a global optimum and can potentially lead to infeasible models [13].

Real-world OTS problems are part of the power system operations model, and the OTS problems have to be solved within the operational time frame. Thus, computational efficiency is extremely important for OTS problems. For large-scale OTS problems, a moderate change in the value of the big M can result in a considerable difference in the computational efficiency. Although the big-M-based OTS model has been widely used [15]-[18], there still lacks a method to search for the optimal value for the big M-based OTS problem.

To fill this gap, this thesis chapter aims to propose a model to find the optimal big M values for the big M-based OTS problems. The contributions of this chapter are as follows. First, an evaluation on the effects of different big M values on the computational efficiency of OTS problems is presented. Second, a model to find the optimal big M values is proposed. The model was implemented on a modified RTS-96 test system with different contingency scenarios, and results show that the proposed model can effectively find the optimal big M values for OTS problems, reducing the solution time of the big M-based OTS problems while achieving optimality and maintaining numerical stability.

The remainder of this chapter is organized as follows. Section 3.3 describes the proposed big M value optimization model for OTS problems. Model setup, cases descriptions, and results discussion is presented in Section 3.4. Finally, Section 3.5 summarizes the main conclusions.

3.3 The Big-M Value Optimization Method

This section presents the proposed big M value optimization model for OTS problems, and the model is presented in equations (3.2)-(3.26). The model is based on a multi-hour OTS model, with M being a variable, while allowing different transmission contingency scenarios to be considered. To better observe the detrimental consequences of an erroneous big M selection, load shedding and wind power curtailment are allowed with a penalty in the model.

$$min\left\{\sum_{t=1}^{T}\left[\mu^{M}M_{t}\right.\right.$$
$$+\sum_{g=1}^{G}\left(\mu_{g}^{NL}u_{g,t}+\mu_{g}^{SD}u_{g,t}^{SD}+\mu_{g}^{SU}u_{g,t}^{SU}+\mu_{g}^{SR}\left(SR_{g,t}^{U}+SR_{g,t}^{D}\right)\right.$$
$$\left.+\sum_{seg=1}^{N}\mu_{g}^{seg}P_{g,t}^{seg}+\sum_{s=1}^{S}\gamma_{t,s}\mu_{g}^{sr}\left(sr_{g,t,s}^{D}+sr_{g,t,s}^{U}\right)\right)$$
$$\left.\left.+\sum_{b=1}^{B}\sum_{s=1}^{S}\gamma_{t,s}\left(\mu_{b}^{FLC}P_{b,t,s}^{FLC}+\mu^{WC}P_{b,t,s}^{WC}\right)\right]\right\} \quad (3.1)$$

$$u_{g,t}P_{g}^{min}\leq P_{g,t}\leq u_{g,t}P_{g}^{max} \quad (3.2)$$

$$0\leq P_{g,t}^{seg}\leq P_{g}^{seg,max} \quad (3.3)$$

$$P_{g,t}=\sum_{seg=1}^{N}P_{g,t}^{seg} \quad (3.4)$$

$$-F_{k}^{max}Z_{k}^{F}Z_{k,t}\leq F_{k,t,s}\leq F_{k}^{max}Z_{k}^{F}Z_{k,t} \quad (3.5)$$

$$-b_{k}\left(\theta_{fr,k,t,s}-\theta_{to,k,t,s}\right)-\left(1-Z_{k,t}\right)M\leq F_{k,t,s} \quad (3.6)$$

$$-b_{k}\left(\theta_{fr,k,t,s}-\theta_{to,k,t,s}\right)+\left(1-Z_{k,t}\right)M\geq F_{k,t,s} \quad (3.7)$$

$$\sum_{k=1}^{K}(1-Z_{k,t})\leq Z_{k}^{max} \quad (3.8)$$

$$\sum_{g\in g_{b}}\left(P_{g,t}+sr_{g,t,s}^{U}-sr_{g,t,s}^{D}\right)+\sum_{k\in\sigma_{b}^{+}}F_{k,t,s}-\sum_{k\in\sigma_{b}^{-}}F_{k,t,s}+P_{b,t,s}^{W}-P_{b,t,s}^{WC}+P_{b,t,s}^{LC}=P_{b,t}^{L} \quad (3.9)$$

$$0\leq M_{t}\leq M_{max} \quad (3.10)$$

$$u_{g,t}^{SU}-u_{g,t}^{SD}=u_{g,t}-u_{g,t-1} \quad (3.11)$$

$$u_{g,t}^{SU}+u_{g,t}^{SD}\leq 1 \quad (3.12)$$

$$\sum_{t=m}^{m+T_{g}^{up-1}}u_{g,t}\geq T_{g}^{up}\left(u_{g,m}-u_{g,m-1}\right),\quad 2\leq m\leq T-T_{g}^{up}+1 \quad (3.13)$$

$$\sum_{t=m}^{m+T_{g}^{down-1}}\left(1-u_{g,t}\right)\geq T_{g}^{down}\left(u_{g,m-1}-u_{g,m}\right),\quad 2\leq m\leq T-T_{g}^{down}+1 \quad (3.14)$$

$$-60R_{g}u_{g,t}\leq P_{g,t}-P_{g,t-1}\leq 60R_{g}u_{g,t} \quad (3.15)$$

$$P_{g,t}-SR_{g,t}^{D}\geq P_{g}^{min}u_{g,t} \quad (3.16)$$

$$P_{g,t} + SR^{U}_{g,t} \leq P^{max}_{g} u_{g,t} \tag{3.17}$$

$$0 \leq SR^{U}_{g,t} \leq 10R_{g} \tag{3.18}$$

$$0 \leq SR^{D}_{g,t} \leq 10R_{g} \tag{3.19}$$

$$0 \leq sr^{U}_{g,t,s} \leq SR^{D}_{g,t} \tag{3.20}$$

$$0 \leq sr^{D}_{g,t,s} \leq SR^{U}_{g,t} \tag{3.21}$$

$$0 \leq P^{WC}_{b,t,s} \leq P^{W}_{b,t,s} \tag{3.22}$$

$$0 \leq P^{FLC}_{b,t,s} \leq P^{L}_{bt} \tag{3.23}$$

$$\theta^{min}_{k} \leq \theta_{fr,k,t,s} - \theta_{to,k,t,s} \leq \theta^{max}_{k} \tag{3.24}$$

$$\theta_{1,t,s} = 0 \tag{3.25}$$

The objective function (3.2) has the goal of minimizing the total cost. Equation (3.2) considers big M as an hourly variable instead of a constant predetermined value. Furthermore, a minor penalty cost is added to the big-M variable to avoid unnecessarily large M values while keeping the generation dispatch cost the dominant objective. Additionally, (3.2) considers the piece-wise linear generation cost, spinning reserve cost, start-up, shutdown, and no-load cost, as well as the load curtailment and wind power curtailment penalties. Generation limits are modeled in (3.3) and the generation piece-wise linear segments constraints are described in (3.4) and (3.5). Equation (3.6) describes the transmission capacity limits considering transmission contingencies and transmission switching. Additionally, Equations (3.7) and (3.8) represent the DC power flow constraints considering a big-M formulation and the maximum permitted transmission line switching is modeled in (3.9). Equation (3.10) describes the nodal power balance constraint and (3.11) sets an upper limit for M. The start-up and shutdown constraints are modeled in Equations (3.12) and (3.13), while Equations (3.14) and (3.15) model the minimum up and down time for the generators. The hourly generation ramp constraint is modeled in (3.16), Equations (3.17) and (3.18) describe the spinning up and down reserves correspondingly. The reserve energy

deployment time is described in Equations (3.19) and (3.20), while the energy deployment limits are shown in Equations (3.21) and (3.22). The wind power curtailment and load curtailment constraints are modeled in Equations (3.23) and (3.24), respectively, and Equations (3.25) and (3.26) are the constraints for the bus voltage angle.

3.4 Case Study, Results, and Discussion

3.4.1 Case Studies and Model Setup

The proposed model was implemented on the RTS-96 test system with a minor modification; two wind energy farms located at bus 3 and bus 24, each with a 200-MW rated power similar to the model in [19]. Two different conditions were used to evaluate the effects of different big M values in the OTS model: (1) One wind power output scenario was considered, and (2) 25 wind power output scenarios were considered. Under each condition, two sub-conditions are considered: (a) No transmission contingency exists in the system; (b) Three highly utilized transmission lines fail in the system. Furthermore, under each sub-condition, three cases were carried out, allowing a maximum of 1, 2, and 3 transmission lines to be switched out, respectively. In total, 12 test cases were carried out. A small penalty cost of $1E-7/unit was added to the M variable in the objective function. Additionally, the load curtailment and wind power curtailment penalties were set at $10,000/MW and $30/MW, respectively. The model proposed in Section III was implemented using a two-step approach. In the first step, the unit commitment variable was solved without considering transmission switching. In the second step, the model was solved with predetermined values for the unit commitment variables, start-up and shut-down variables.

3.4.2 The Impact of the Big-M Value on the Objective Function

Choosing an extremely large or a small value of M can have undesirable consequences to the optimization problem [9]. To study the impact of the big M value on the objective value, the OTS model in Section III was solved using predetermined values of M without the penalty for the big M. The M values used in this study ranged from 1E2 to 1E12 for the 1-scenario cases and from 1E2 to 1E9 for the 25-scenario cases. The big M values in the latter cases were smaller because the problem became very computationally burdensome with such large M values, and we only chose cases that could be solved within 7200 seconds. The objective values of different cases obtained with different big M values are shown in Fig. 3.1 and Fig. 3.2.

From the two figures, it can be seen that, with a small value of M (less than 10E3), the search space for the solution was limited, thus the OTS problem could not converge to the global optimum. With an excessively large M value (greater than 10E7), unreasonable objective values were produced because of the numerical instability. Thus, the values of the big M have to be chosen properly to avoid instability in the optimization model [20].

3.4.3 The Optimal M Model

Using the model proposed in Section III, the optimal values of the big M were solved for 24 hours in the 12 cases described in section IV.A, and the optimal big M values are shown in Fig. 3.3 and Fig. 3.4. It can be observed that the optimal big M values vary with time, the maximum number of lines to be switched, and transmission contingencies.

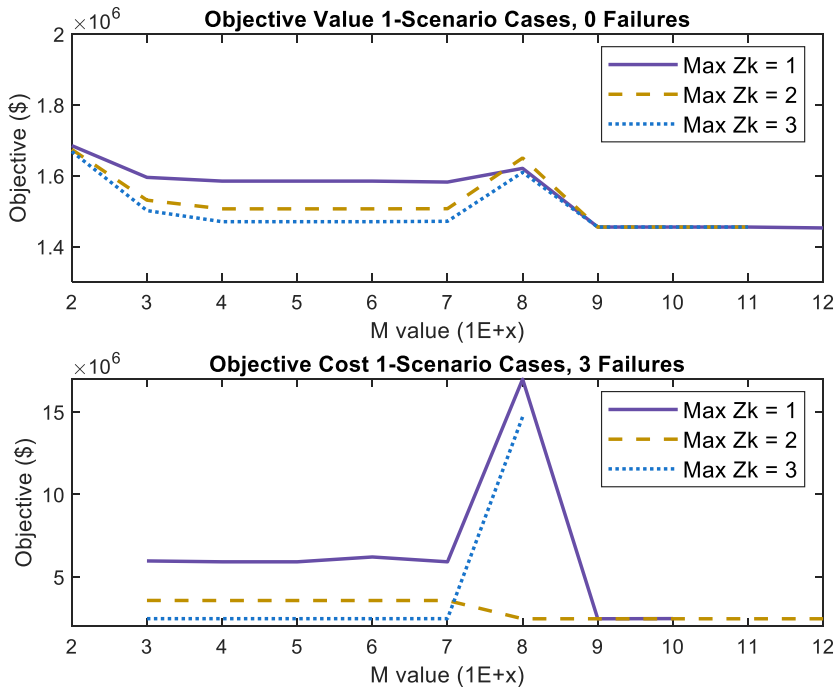

Figure 3.1: Objective Value for the 1-Scenario Cases under different M values

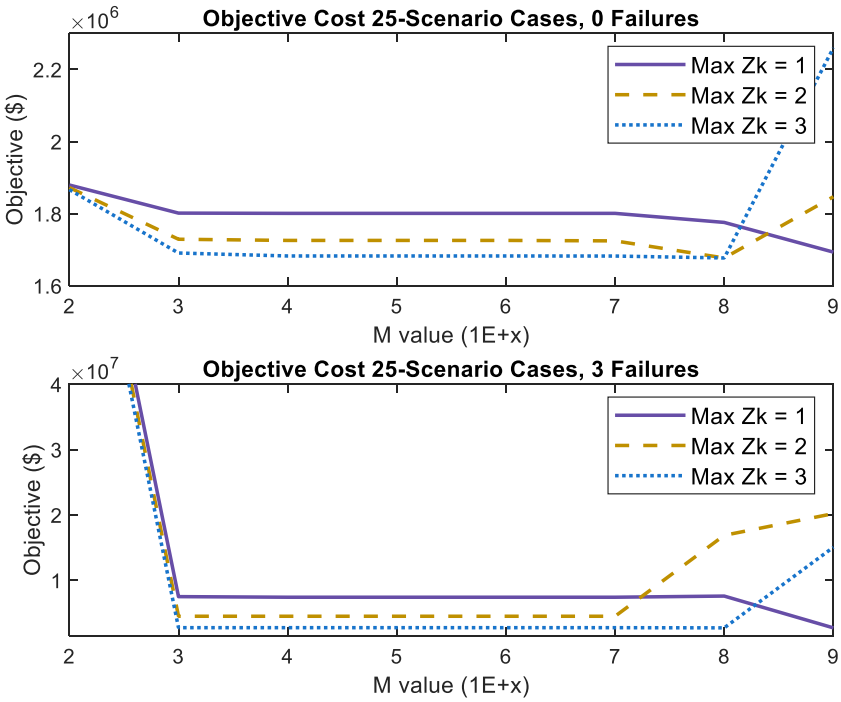

Figure 3.2: Objective Value for the 25-Scenario Cases under different M values

3.4.2 Computational Efficiency

To study the impact of big M values on the computational efficiency of the OTS model, the solution time of the OTS cases were obtained with the M values being 1000, 5000, 10000, and the obtained optimal M values for each of the 12 cases. The solution times for the 1-scenario and 25-scenario cases are listed in Table 3.1 and Table 3.2, respectively. The cases were implemented using Python and Gurobipy on a computer with an Intel Core i7-1065G7 CPU and 16GB of RAM.

From Table 3.1 and Table 3.2 it can be observed that in most of the cases the computational time increased with the increase of the M values. With the optimal M values, the solution time was always the shortest among the cases where the global optimum could be reached under each condition. This verifies the effectiveness of the proposed model in obtaining optimal big M values for OTS problems.

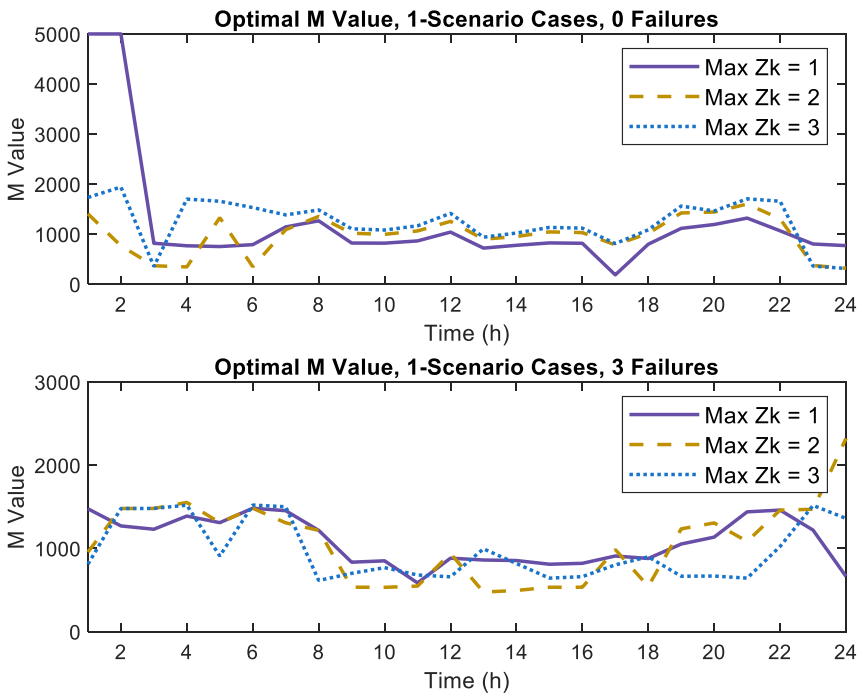

Figure 3.3: Optimal M Values for the 1-Scenario Cases

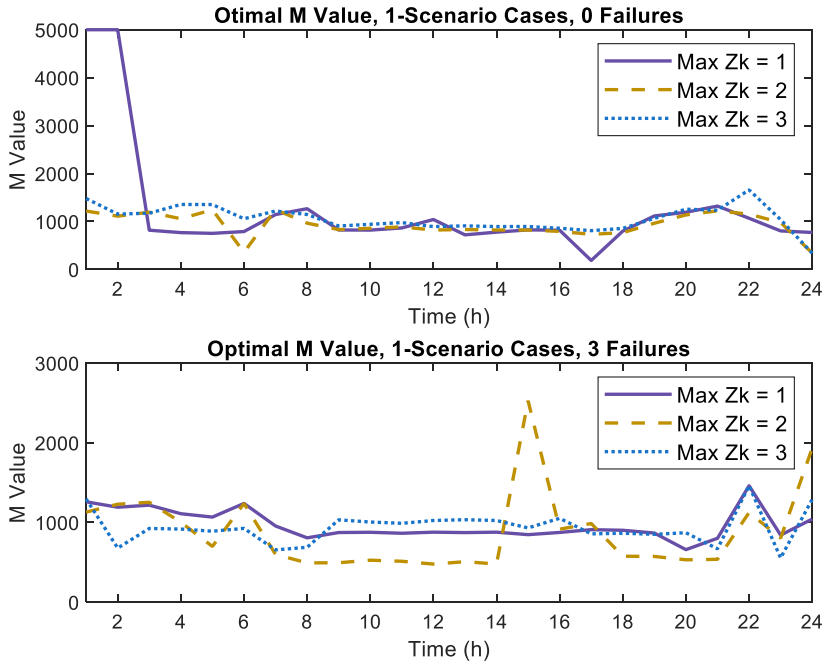

Figure 3.4: Optimal M Values for the 25-Scenario Cases

3.5 CONCLUSIONS

This chapter proposes a big M value optimization model for big M-based OTS problems and evaluates the impact of the big M values on the optimality and computational efficiency of the OTS problems. The model was implemented on a modified RTS-96 test system under 12 conditions. The results presented in Table 3.1 and Table 3.2 show that properly chosen big M values are critical to the computational efficiency, optimality, and stability of the OTS problems, and the proposed model can effectively find a set of optimal values for the big M, allowing the OTS problem to be solved fast while converging to the global optimum.

Table 3.1: Computational Times for 1-Scenario OTS

M	*1000*	*5000*	*10000*	*Optimal M*
	1 Transmission Switch Allowed – No failures			
Time (s)	3.157	3.355	3.376	3.063
Objective ($)	1,595,271	1,584,756	1,584,756	1,584,756
	1 Transmission Switch Allowed – 3 failures			
Time(s)	2.266	2.567	2.703	2.008
Objective ($)	5,964,818	5,911,480	5,911,480	5,911,480
	2 Transmission Switch Allowed – No failures			
Time(s)	4.235	4.579	5.547	4.207
Objective ($)	1,530,968	1,506,473	1,506,473	1,506,473
	2 Transmission Switch Allowed – 3 failures			
Time(s)	2.938	3.360	3.579	2.859
Objective ($)	3,569,559	3,564,907	3,564,907	3,564,907
	3 Transmission Switch Allowed – No failures			
Time(s)	7.097	6.646	7.754	5.709
Objective ($)	1,501,527	1,470,217	1,470,217	1,470,217
	3 Transmission Switch Allowed – 3 failures			
Time(s)	3.391	4.016	4.126	3.193
Objective ($)	2,465,004	2,464,802	2,464,802	2,464,802

Table 3.2: Computational Times for 25-Scenario OTS

M	*1000*	*5000*	*10000*	*Optimal M*
	1 Transmission Switch Allowed – No failures			
Time(s)	162.617	260.895	249.264	158.593
Objective ($)	1,801,245	2,464,802	2,464,802	2,464,802
	1 Transmission Switch Allowed – 3 failures			
Time(s)	63.322	132.663	135.299	52.653
Objective ($)	7,489,953	7,399,367	7,399,367	7,399,367
	2 Transmission Switch Allowed – No failures			
Time(s)	149.566	195.236	203.369	192.162
Objective ($)	1,728,716	1,725,476	1,725,476	1,725,476
	2 Transmission Switch Allowed – 3 failures			
Time(s)	106.641	113.697	130.817	85.121817
Objective ($)	4,489,102	4,488,312	4,488,312	4,488,312
	3 Transmission Switch Allowed – No failures			
Time(s)	186.261	252.698	266.511	216.309
Objective ($)	1,690,485	1,682,310	1,682,310	1,682,310
	3 Transmission Switch Allowed – 3 failures			
Time(s)	112.588	125.534	139.057	121.698
Objective ($)	2,739,361	2,739,222	2,739,222	2,739,222

3.6 REFERENCES

[1] A. Tuohym and P. Meibom, "Unit commitment for systems with significant wind penetration," IEEE Transactions on Power Systems, vol. 24, no. 2, pp. 592-601, 2009.

[2] B. C. Ummels, M. Gibescu, E. Pelgum, “Impacts of wind power on thermal generation unit commitment and dispatch,” IEEE Transactions on Energy Concersions, vol. 22, no. 1, pp. 44-51, 2007.

[3] K. W. Hedman, S. S. Oren, and R. P. O’Neil, “Optimal transmission switching: economic efficiency and market implications,” Journal of Regulatory Economics, vol. 40, no.2, pp. 111-140, 2011.

[4] E. B. Emily, R. P. O’Neil, and M. C. Ferris, “Optimal transmission switching,” I EEE Transactions of Power Systems, vol. 23, no. 3, pp. 1346-1355, 2008.

[5] W. Shao and V. Vittal, “BIP-based OPF for line and bus-bar switching to relieve overloads and voltage violations,” IEEE Power Systems Conference and Exposition, pp. 2090–2095, 2006.

[6] W. Shao and V. Vittal, “A new algorithm for relieving overloads and voltage violations by transmission line and bus-bar switching,” IEEE PES Power Systems Conference and Exposition, pp. 322-327. 2004

[7] R. Bacher and H. Glavitsch, “Network topology optimization with security constraints,” IEEE Transactions on Power Systems, vol. 1, no. 4, pp. 103-111, 1986.

[8] G. Schnyder and H. Glavitsch, “Integrated security control using an optimal power flow and switching concepts,” IEEE Transactions on Power Systems, vol. 3, no. 2, pp. 782-790, 1988.

[9] S. Fattahi, J, Lavaei, and A. Atamturk, “A bound strengthening method for optimal transmission switching in power systems,” IEEE Transactions on Power Systems, vol. 43, no. 1, pp. 280-291, 2018.

[10] G. Codato and M. Fischetti, "Combinatorial Benders’ cuts for mixed-integer linear programming," Operations Research, vol. 54, no. 4, pp. 756-766, 2006.

[11] J. D. Camm, A. S. Raturi, and S. Tsubakitani, "Cutting big M down to size," Interfaces, vol. 20, no. 5 pp. 61-66, 1990.

[12] T. Ding, R. Bo, F. Li, and H. Sun, “Optimal power flow with the consideration of flexible transmission line impedance,” IEEE Transactions on Power Systems, vol. 31, no. 2, pp. 1655-1656, 2015.

[13] M. Cococcioni, and L. Fiaschi, "The Big-M method with the numerical infinite M," Optimization Letters, vol. 15, no. 7, pp. 2455-2468, 2021.

[14] T. Ding, R. Bo, F. Li, and H. Sun, “Big-M based MIQP method for economic dispatch with disjoint prohibited zones,” IEEE Transactions on power systems, vol. 29, no. 2, pp. 976-977, 2013.

[15] R. P. O’Neill, P. Richard, K. W. Hedman, E. A. Krall, A. Papavasiliou, and S.S. Oren, “Economic analysis of the N-1 reliable unit commitment and transmission switching problem using duality concepts,” Energy Systems, vol. 1, no. 2, pp.165-195, 2010.

[16] J. Ostrowski, J. Wang, and C. Liu, “Exploiting symmetry in transmission lines for transmission switching,” IEEE Transactions on Power Systems, vol. 27, no. 3, pp. 1708-1709, 2012.

[17] C. Liu, J. Wang, and J. Ostrowski, “Heuristic prescreening switchable branches in optimal transmission switching,” IEEE Transactions on Power Systems, vol. 27, no. 4, pp. 2289-2290, 2012.

[18] T. Ding and C. Zhao, “Robust optimal transmission switching with the consideration of corrective actions for N-k contingencies,” IEEE Generation, Transmission & Distribution, vol. 10, no. 13, pp. 3288-3295, 2016.

[19] Y. Sang, M. Sahraei-Ardakani and M. Parvania, "Stochastic Transmission Impedance Control for Enhanced Wind Energy Integration," IEEE Transactions on Sustainable Energy, vol. 9, no. 3, pp. 1108-1117, July 2018.

[20] Gurobi, Dealing with big-M constraints. Accessed on: Nov. 7, 2021. [Online]. Available: https://www.gurobi.com/documentation/9.1/refman/dealing_with_big_m_constra.html

Chapter 4: Decentralized Consensus-ADMM Decision-Making

One of the main challenges of power systems resiliency is its ability to withstand and reduce load loss under natural disasters. Additionally, the variability of resources across the network and the introduction of RESs is forcing the grid to depend at a higher level in interconnections and the electricity market. Besides the economic goals of a power system, reliability is the number one consideration and the main focus towards grid modernization. This section includes a published paper comparing the power system resiliency of a centralized versus a decentralized decision-making algorithm by evaluating the load loss on both cases.[2]

Natural disasters have been causing an increasing amount of economic losses in the past two decades. Natural disasters, such as hurricanes, winter storms, and wildfires, can cause severe damages to power systems, significantly impacting industrial, commercial, and residential activities, leading to not only economic losses but also inconveniences to people's day-to-day life. Improving the resilience of power systems can lead to a reduced number of power outages during extreme events and is a critical goal in today's power system operations. This chapter presents a model for decentralized decision-making in power systems based on distributed optimization and implemented it on a modified RTS-96 test system, discusses the convergence of the problem, and compares the impact of decision-making mechanisms on power system resilience. Results show that a decentralized decision-making algorithm can significantly reduce power outages when part of the system is islanded during severe transmission contingencies. .

4.1 NOMENCLATURE

Indices

b	Bus.
g	Generator.
k	Iteration number.
l	Transmission line.
seg	Segments for piece-wise linear cost function.

[2] Reprinted with permission from L. Ramirez-Burgueno, Y. Sang, and N. Santiago, "Improving Power System Resiliency through Decentralized Decision-Making," *IEEE*

Sets

σ_b^+ Transmission lines with their "to" bus connected to bus b.

σ_b^- Transmission lines with their "from" bus connected to bus b.

g_b Generators connected to bus b.

Variables

θ_b Voltage angle of bus.

$\theta_{fr,l}$ Voltage angle at the "from" bus of line l.

$\theta_{to,l}$ Voltage angle at the "to" bus of line l.

P_g Real power generation of generator g.

P_g^{seg} Real power generation of generator g in segment seg.

P_b^{LC} Flexible load curtailment of bus b.

F_l Real power flow through transmission line l

Parameters

θ_k^{min} Minimum voltage angle difference at line l.

θ_k^{max} Maximum voltage angle difference at line l.

θ_1 Voltage angle at the slack bus at time t.

B Total number of buses.

B_b The set of indices for subproblems that include θ_b.

B_e The set of indices for the buses that are connected to tie lines in subproblem e.

B_i The total number of buses in subproblem i.

b_l Susceptance of transmission line l.

G Total number of generators.

G_i Total number of generators in area i.

P_b^L Load at bus b.

F_l^{max} Upper real power flow limit of transmission line l.

F_l^{min} Lower real power flow limit of transmission line l.

N Number of piece-wise linear segments for the generators.

P_g^{max} Upper generation limit of generator g.

P_g^{min} Lower generation limit of generator g.

$P_g^{seg,max}$ Upper generation limit of generator g in segment seg.

θ_b^a The average value of θ_b from all the distributed optimization problems that include θ_b.

μ_g^{seg} Linear cost of generator g in segment seg.

μ_b^{LC} Flexible load curtailment compensation rate for bus b.

ρ The ADMM step size.

λ_b^k Penalty value for θ_b at iteration k.

ε Optimality gap.

4.2 INTRODUCTION

Natural disasters have caused significant economic losses throughout the history, and the power outages caused by natural disasters is one of the leading causes of economic losses [1]. The economic losses caused by power outages including the revenue lost for utility companies, direct or indirect losses from electricity customers, such as the interruption of industrial and commercial activities, and inconvenience in the electricity customer's daily life [2]. In recent years, natural disasters have caused significant power outages throughout the U.S. In 2017, Hurricanes Harvey, Irma, and Maria caused significant damages to power systems in multiple states, including Texas, Florida, and Puerto Rico, and led to long-lasting power outages, especially in Puerto Rico, which lasted for several months [3]-[6]. In 2018, Hurricanes Florence and Michael made U.S. landfalls and affected more than 1 million electricity customers [7], [8]. In 2019, Hurricanes Dorian and Barry caused power outages to at least half a million electricity customers [9], [10], and in 2020, Hurricanes Isaias, Laura, Sally caused power outages to millions of electricity customers in multiple states, including New York, New Jersey, Connecticut, Louisiana, Alabama, Georgia, and Florida [11]-[13]. In 2021, a winter storm hit Texas, in which 4.5 million homes lost power, causing billions of dollars of losses and the death of 57 people [14]. History has shown the significant impact of power outages on the society, and, thus, it is critical to improve the resilience of power systems. Different natural disasters can cause damages to different parts of power systems. Hurricanes can cause damages to transmission and distribution lines and flooding in power plants [3]-[13]. Winter storms can freeze transmission and distribution lines, fuel pipes for power plants, or wind turbines [14]. Wildfires can damage power plants, transmission, and distribution lines. Thus, different measures need to be taken to cope with different natural disasters [15]. In this study, we specifically focus on damages caused to transmission lines, especially severe

damages of transmission systems that island part of the power system. This is because transmission lines can be damaged by different types of natural disasters and are one of the most commonly seen components damaged by natural disasters, and unlike the damage of distribution lines, which usually causes local power outages, the damage of transmission systems can cause widespread outages in the system. There are a number of methods that can be used to improve power system resilience by addressing transmission system failures. From a time-scope perspective, the methods can be divided into three categories [16], [17]. The first category includes preventive measures taken during the planning process, which happens years before the system is committed. This mainly includes system hardening, such as building strong transmission poles or use underground lines [18]. The second category is preventive operational decision-making, which happens from months to minutes before the extreme events. This includes preparing enough onsite fuel storage at certain power plants, pre-allocating the maintenance crew to vulnerable locations, and decide the unit commitment and generation dispatch during the extreme event [16], [19]-[24]. The third category of methods are for the restoration after the extreme events. This mainly includes the dispatch of restoration crew, the sequence of component restoration, etc. [25]-[30]. The U.S. has an aging transmission system and upgrading the transmission system is an extremely capital-intensive and time-consuming process. To reduce power outages during natural disasters, the second category of methods, preventive operation, plays an important role. Reference [19] proposes a method to pre-allocate resources for restoration, which can be considered as a preventive measure. Reference [16] proposed a preventive operation method which considers possible contingency scenarios based on weather forecast. This method can reduce power outages and over generation without over committing generation resources, and this method works well for interconnected systems. However, some natural disasters cause such severe damage that part

of the power system is islanded from the rest. In such cases, damaged were not only the transmission lines but also the communication equipment. Due to this reason, control signals cannot be sent from the control center to the islanded area, and the control center cannot remotely monitor the conditions of the components in the islanded area, causing difficulties in operating system in islanded area and resulting in severe power outages. To fill this gap, this chapter proposes a decentralized decision-making method based on distributed optimization. This method enables decentralized decision-making in different areas of power systems. When the areas are interconnected, a consensus will be achieved by all the participating areas. When one or more areas are islanded, the islanded area will be able to make decisions on their own while the remaining interconnected areas make decisions by achieving a consensus. The method was implemented on a modified RTS-96 test system, and results show that the decentralized decision-making method can significantly reduce power outages compared to a centralized decision-making method.

The remaining sections of the chapter are organized as follows. Section 4.3 presents the distributed optimization model used in this study. A case study is discussed in Section 4.4, and conclusions are drawn in Section 4.5.

4.3 MATHEMATICAL MODEL

In this thesis chapter, we used both the centralized and decentralized decision-making methods to decide generation dispatch in case of severe contingencies caused by natural disasters. The two decision-making models are presented as follows.

4.3.1 Centralized Decision Making

The centralized decision-making model is based on a DCOPF model [31] and presented by Equations (4.1)-(4.10). Using this model, only one control center is needed for a power system, and control signals can be sent to different components in the system that need to be operated. The advantage of this method is that it is easy to implement, and the disadvantage of this method is

that when one area in the power system is islanded due to severe contingencies, the load in this area will be completely lost because control signals cannot be sent to the area. The model allows load loss, but the load loss is penalized with a high cost in the objective function, as Equation (4.1) shows. Besides the penalty for the load loss, the generation dispatch cost is also included in the objective function, and a piece-wise linear generation cost is adopted. Equation (4.2) is the nodal power balance constraint, which allows load loss. Equations (4.3)-(4.5) are the generation constraints considering the piece-wise linear segments. Equations (4.6) and (4.7) are the power flow constraints. The maximum load loss cannot exceed the maximum load at the bus, as Equation (4.8) shows. Since the DCOPF model can only be applied when the differences between bus voltages angles are small, Equation (4.9) sets a limit for the bus voltage angle differences between the two ends of each transmission line, and Equation (4.10) sets Bus 1 as the reference bus.

$$\min\left\{\sum_{g=1}^{G}\sum_{seg=1}^{N}\mu_g^{seg}P_{g,t}^{seg}+\sum_{b=1}^{B}\mu^{LC}P_b^{LC}\right\} \tag{4.1}$$

$$\sum_{g\in g_b}P_g+\sum_{l\in\sigma_b^+}F_l-\sum_{l\in\sigma_b^-}F_l=P_b^L-P_b^{LC} \tag{4.2}$$

$$P_{g,t}=\sum_{seg=1}^{N}P_{g,t}^{seg} \tag{4.3}$$

$$0\le P_{g,t}\le P_g^{max} \tag{4.4}$$

$$0\le P_{g,t}^{seg}\le P_g^{seg,max} \tag{4.5}$$

$$-b_l\left(\theta_{fr,l}-\theta_{to,l}\right)=F_l \tag{4.6}$$

$$F_l^{min}\le F_l\le F_l^{max} \tag{4.7}$$

$$0\le P_b^{LC}\le P_b^L \tag{4.8}$$

$$\theta_l^{min}\le\theta_{fr,l}-\theta_{to,l}\le\theta_l^{max} \tag{4.9}$$

$$\theta_1=0 \tag{4.10}$$

4.3.2 Decentralized Decision-Making Based on ADMM

The decentralized decision-making algorithm is based on a distributed DCOPF, which is developed using the alternating direction method of multipliers (ADMM) [32], [33]. ADMM is

adopted in study because it is suitable for parallelize the power system optimization problem based on sub-areas of the power system. The decentralized decision-making algorithm allows us to divide the power system into multiple areas and make generation dispatch decisions in a decentralized manner based on areas. Using this algorithm, each area needs to have a control center, and the control centers communicate with each other to reach a consensus on generation dispatch decisions. In this way, globally optimal generation dispatch decisions can be made. When one of the areas is islanded, the area will operate independently and make locally optimal decisions for the area, while the interconnected areas could still communicate and make globally optimal decisions. When one area of the system is islanded, the area could still make sure at least some of the load in this area being met, thus reducing load loss caused by such islanding events. To implement this algorithm, each area needs to implement a distributed optimization problem, or subproblem. For these subproblems, only the bus voltage angles at the two ends of the tie lines between different areas need to reach a consensus. Other variables in the optimization problems are internal to each area and does not need to be agreed on by other areas. The objective function of the distributed optimization problem is shown in Equation (4.11). It minimizes the total generation dispatch cost in the area, penalizes load loss in the area, and includes two ADMM terms that facilitates the consensus-reaching process of certain variables. Constraints (4.2)-(4.10) will be included in each distributed optimization problem, however, the constraints in each problem will only consider the generators, transmission lines, and buses in each area. The global optimal solution will be achieved in an iterative manner. In each iteration, all the subproblems need to be solved, and then the bus voltage angles at the ends of tie lines will be exchanged between different subproblems. An average of each variable that needs to be agreed on is calculated by Equation (4.12), and then the Lagrangian multipliers will be updated using Equation (4.13). A flow chart for the solution process is shown in Fig. 4.1.

$$\min_{P^{k+1},\theta^{k+1}} \left\{ \begin{aligned} &\sum_{g=1}^{G_i} \sum_{seg=1}^{N} \mu_g^{seg} P_{g,t}^{seg,k+1} + \sum_{b=1}^{B_i} \mu^{LC} P^{LC} \\ &+ \sum_{b=1}^{B_e} \lambda_b^k (\theta_b - \theta_b^a) + \sum_{b=1}^{B_e} \frac{\rho}{2} \|\theta_b - \theta_b^a\|_2^2 \end{aligned} \right\} \tag{4.11}$$

$$\theta_b^a = \frac{1}{B} \sum_{b=1}^{B_b} \theta_b \tag{4.12}$$

$$\lambda_b^{k+1} = \lambda_b^k + \rho(\theta_b - \theta_b^a) \tag{4.13}$$

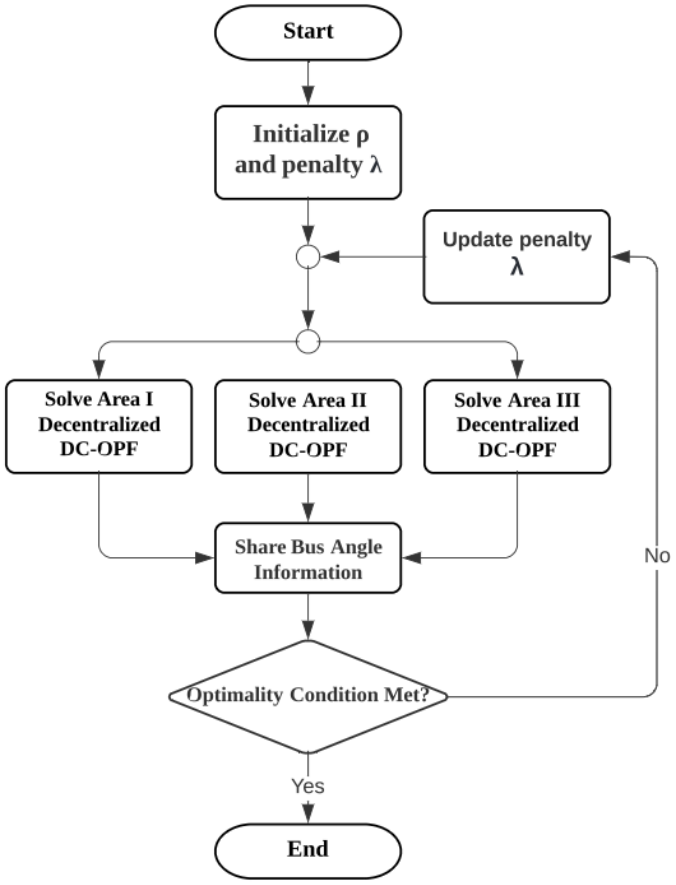

Figure 4.1: Decentralized Consensus-ADMM Algorithm Flowchart

4.4 Case Studies and Results Discussion

4.4.1 Simulation Setup

A modified version of the RTS-96 test system [34] was used to implement the case studies of the proposed simulations, and each case study is implemented in single-period manner. For case study purposes, the mentioned 24-bus system was divided into three sub-regions or areas as presented in Table 4.1. In this case study, the areas were divided in a way that minimizes the number of tie-lines between regions and consequently reduce the computational time for the decentralized model. The area division and node clustering can be optimally performed with assistance of graph theory clustering methods [35].

This case study was implemented assuming Area III is islanded from the other areas due to the outage of all the tie lines that connects Area III to other areas. The resilience study evaluates load-loss results under this condition when the system was operating in centralized and decentralized cases. In the centralized case, the control center was assumed to be in Area I, and in the decentralized case, there was a sub-control center in each area.

Table 4.1: RTS-96 Case Study Areas

	Buses	*Available Generation Capacity (MW)*	*Load*
Area I	1 – 7, 24	684	791
Area II	8 – 13	591	1286
Area III	14 – 23	2130	773

4.4.2 Centralized Decision-Making Results

The centralized decision making was implemented using the model shown in Section 4.3.1, when the control center was located in Area I and Area III was islanded. When Area III was islanded, no power lines or communication wires were connecting Area I and Area II with Area III, and thus neither power nor control signals could be delivered to Area III. Results from the centralized decision-making algorithm are shown in Table 4.2.

Table 4.2: Load loss in centralized decision-making

	Load (MW)	*Generation (MW)*	*Load Loss(MW)*
Area I & II	2,077	1,275	802
Area III	773	0	773
Total Load Loss			**1,575**

As the results show, with no control signal from the centralized control center and all the tie lines out, Area III could neither generate power for itself nor receiving power from other areas, and this resulted in a significant amount of load loss, which totals 1,575 MW. Islanding Area III can be considered as the worst islanding contingency scenario, due to the inability of Area I and Area II to fulfill its demand. Areas I and II had a total load loss of 802 MW because of a lack of generation capacity. The importance of implementing distributed control can be noted in this scenario, where although enough generation was present to meet the local area demand in Area III, the control signals could not be sent properly due to communication failures, resulting in a complete load loss in Area III.

4.4.3 Decentralized Decision-Making Results

The To overcome the problems caused by a single centralized control center, the distributed algorithm shown in section 4.3.2 was implemented to simulate distributed control centers in each area. This case allowed Area I and Area II to exchange power and bus voltage angle information, with the advantage that the islanded Area III could make its own generation dispatch decisions. Area I and II shared bus voltage angle information to reach a consensus, while Area III operates independently. The results are provided in Table 4.3.

Table 4.3: Load loss in decentralized decision-making

	Load (MW)	*Generation (MW)*	*Load Loss(MW)*
Area I & II	2,077	1,275	802
Area III	773	773	0
Total Load Loss			**802**

Results from Area I and Area II remain consistent with the centralized algorithm, however, since Area III could perform decision-making independently in this case, load loss in Area III is eliminated since Area III has enough generation capacity. Since Area III is able to meet its total load demand through independent decision-making, the total load loss reduced by 51% compared to case with centralized decision-making. .

4.4.4 Computational Efficiency

Both centralized and decentralized algorithms were implemented using Python and Gurobipy on a Computer with an Apple M1 Pro CPU and 16 GB of RAM. The computational time for the centralized algorithm was 0.28 seconds, compared to the decentralized algorithm taking 41.13 seconds to converge. Although the decentralized version took considerably longer than the centralized version, both solutions could be found within an appropriate operational time frame. .

4.5 CONCLUSIONS

This chapter presents an ADMM-based distributed DCOPF model which allows load loss during emergent conditions and studies the importance of decentralized algorithms and the positive effects of decentralized control when severe contingencies island part of the power system. The ADMM-based distributed DCOPF algorithm was implemented on a modified RTS-96 test system when severe contingencies islands one of the three areas. Results show that the decentralized decision-making method can significantly reduce the total load loss under extreme events in which communication and power interconnections are interrupted. In the future work, the decentralized

decision-making algorithm will be tuned to speed up its convergence and apply to large-scale power systems with complex operating conditions and different contingency scenarios.

4.6 REFERENCES

[1] "2021 U.S. billion-dollar weather and climate disasters in historical context," NOAA [Online]. Available: https://www.climate.gov/news-features/blogs/beyond-data/2021-us-billion-dollar-weather-and-climate-disasters-historical

[2] S. Mao, C. Wang, S. Yu, H. Gen, J. Yu, H. Hou, "Review on Economic Loss Assessment of Power Outages," Procedia Computer Science, vol. 130, pp. 1158-1163, 2018.

[3] "Hurricane Harvey Event Analysis Report," North American Electric Reliability Corporation, Aug. 2018.

[4] "Hurricane Irma Event Analysis Report," North American Electric Reliability Corporation, Aug. 2018.

[5] U.S. Department of Energy, Infrastructure Security and Energy Restoration, Hurricanes Maria, Irma, and Harvey September 22 Afternoon Event Summary (Report 43).

[6] "Energy Resilience Solutions for the Puerto Rico Grid," The U.S. Department of Energy, June 2018 [Online]. Available: https://www.energy.gov/sites/prod/files/2018/06/f53/DOE%20Report_Energy%20Resilience%20Solutions%20for%20the%20PR%20Grid%20Final%20June%2018.pdf

[7] "Hurricane Florence power outages top 890,000, could hit 3 million as storm unleashes fury," USA Today [Online]. Available: https://www.usatoday.com/story/news/nation/2018/09/14/hurricane-florence-power-outages/1301060002/

[8] “Hurricane Michael caused 1.7 million electricity outages in the Southeast United States,” The U.S. Energy Information Administration (EIA) [Online]. Available: https://www.eia.gov/todayinenergy/detail.php?id=37332

[9] “Hurricane Barry Situation Reports,” The U.S. Department of Energy (DOE) [Online]. Available: https://www.energy.gov/ceser/hurricane-barry-situation-reports-0

[10] “Hurricane Dorian: More than 230000 without power in SC,” Charlotte Observer [Online]. Available: https://www.charlotteobserver.com/article234733197

[11] “Power outages after Tropical Storm Isaias were a warning to utilities,” The Verge [Online]. Available: https://www.theverge.com/21361751/tropical-storm-isaias-power-outages-tristate-utilities-energy-grid

[12] “Power Outage Repairs in Louisiana After Hurricane Laura Cost Up to $1.4 Billion,” The Weather Channel [Onine]. Available: https://weather.com/news/news/2020-09-24-hurricane-laura-power-outages-billion-dollars-entergy

[13] “Hurricane Sally power outages top 540,000 in Alabama, Florida and Georgia,” Fox Business [Online]. Available: https://www.foxbusiness.com/energy/hurricane-sally-power-outage-alabama-florida-georgia-storm-flooding-weather

[14] Carey W. King et. al., “The Timeline and Events of the February 2021 Texas Electric Grid Blackouts,” The University of Texas at Austin Energy Institute, Austin, TX, July 2021 [Online]. Available: https://energy.utexas.edu/ercot-blackout-2021

[15] M. Nazemi and P. Dehghanian, "Powering Through Wildfires: An Integrated Solution for Enhanced Safety and Resilience in Power Grids," IEEE Transactions on Industry Applications, vol. 58, no. 3, pp. 4192-4202, May-June 2022.

[16] Y. Sang, J. Xue, M. Sahraei-Ardakani and G. Ou, "An Integrated Preventive Operation Framework for Power Systems During Hurricanes," IEEE Systems Journal, vol. 14, no. 3, pp. 3245-3255, Sept. 2020.

[17] M. Mahzarnia, M. P. Moghaddam, P. T. Baboli and P. Siano, "A Review of the Measures to Enhance Power Systems Resilience," IEEE Systems Journal, vol. 14, no. 3, pp. 4059-4070, Sept. 2020.

[18] A. Arab, E. Tekin, A. Khodaei, S. K. Khator, and Z. Han, "System Hardening and Condition-Based Maintenance for Electric Power Infrastructure Under Hurricane Effects," IEEE Trans. Reliab., vol. 65, no. 3, pp. 1457–1470, Sep. 2016.

[19] E. Byon, L. Ntaimo, and Y. Ding, "Optimal Maintenance Strategies for Wind Turbine Systems Under Stochastic Weather Conditions," IEEE Trans. Reliab., vol. 59, no. 2, pp. 393–404, Jun. 2010.

[20] C. M. Rocco, J. E. Ramirez-Marquez, D. E. Salazar, and C. Yajure, "Assessing the Vulnerability of a Power System Through a Multiple Objective Contingency Screening Approach," IEEE Trans. Reliab., vol. 60, no. 2, pp. 394–403, Jun. 2011.

[21] C. Wang, Y. Hou, F. Qiu, S. Lei, and K. Liu, "Resilience Enhancement With Sequentially Proactive Operation Strategies," IEEE Trans. Power Syst., vol. 32, no. 4, pp. 2847–2857, 2017.

[22] N. Yodo, P. Wang, and Z. Zhou, "Predictive Resilience Analysis of Complex Systems Using Dynamic Bayesian Networks," IEEE Trans. Reliab., vol. 66, no. 3, pp. 761–770, Sep. 2017.

[23] M. Sahraei-Ardakani and G. Ou, "Day-Ahead Preventive Scheduling of Power Systems During Natuaral Hazards via Stochastic Optimization," in Proc. IEEE PES General Meeting, Chicago, IL, 2017, pp. 1–5.

[24] Y. Sang, M. Sahraei-Ardakani, J. Xue, and G. Ou, "Effective Scenario Selection for Preventive Stochastic Unit Commitment during Hurricanes," in Proc. 2018

IEEE International Conference on Probabilistic Methods Applied to Power Systems (PMAPS), 2018, pp. 1–6.

[25] A. Arab, A. Khodaei, Z. Han, and S. K. Khator, “Proactive recovery of electric power assets for resiliency enhancement,” IEEE Access, vol. 3, pp. 99–109, 2015.

[26] A. Arab, A. Khodaei, S. K. Khator, K. Ding, V. A. Emesih, and Z. Han, “Stochastic pre-hurricane restoration planning for electric power systems infrastructure,” IEEE Trans. Smart Grid, vol. 6, no. 2, pp. 1046–1054, 2015.

[27] P. Van Hentenryck and C. Coffrin, “Transmission system repair and restoration,” Math. Program., vol. 151, no. 1, pp. 347–373, 2015.

[28] C. Coffrin and P. Van Hentenryck, “Transmission system restoration with co-optimization of repairs, load pickups, and generation dispatch,” Int. J. Electr. Power Energy Syst., vol. 72, pp. 144–154, 2015.

[29] A. Golshani, W. Sun, Q. Zhou, Q. P. Zheng, and J. Tong, “Two-Stage Adaptive Restoration Decision Support System for a Self-Healing Power Grid,” IEEE Trans. Ind. Inform., vol. 13, no. 6, pp. 2802–2812, Dec. 2017.

[30] Y. Fang, N. Pedroni, and E. Zio, “Resilience-Based Component Importance Measures for Critical Infrastructure Network Systems,” IEEE Trans. Reliab., vol. 65, no. 2, pp. 502–512, Jun. 2016.

[31] B. Stott, J. Jardim and O. Alsac, "DC Power Flow Revisited," IEEE Transactions on Power Systems, vol. 24, no. 3, pp. 1290-1300, Aug. 2009.

[32] M. Javadi, A. E. Nezhad, M. Gough, M. Lotfi and J. P. S. Catalão, "Implementation of Consensus-ADMM Approach for Fast DC-OPF Studies," in Proc. 2019 International Conference on Smart Energy Systems and Technologies (SEST), 2019, pp. 1-5.

[33] D. Biagioni, P. Graf, X. Zhang, A. S. Zamzam, K. Baker and J. King, "Learning-Accelerated ADMM for Distributed DC Optimal Power Flow," IEEE Control Systems Letters, vol. 6, pp. 1-6, 2022.

[34] Y. Sang, M. Sahraei-Ardakani and M. Parvania, "Stochastic Transmission Impedance Control for Enhanced Wind Energy Integration," IEEE Transactions on Sustainable Energy, vol. 9, no. 3, pp. 1108-1117, July 2018.

[35] I. Gammoudi, M.A. Mahjoub, F. Guerdelli, “Unsupervised Image Segmentation based Graph Clustering Methods,” Computacion y Sistemas, vol. 24, no. 3, pp. 969-987, Sep. 2020.

Glossary

ADMM: Alternating Direction Method of Multipliers

AI: Artificial Intelligence

ANN: Artificial Neural Network

CAISO: California Independent System Operator

DCOPF: Direct Current Optimal Power Flow

DER: Distributed Energy Resources

FR: Flexible Ramp

GHG: Green House Gasses

LMP: Locational Marginal Price

MISO: Midcontinent Independent System Operator

OTS: Optimal Transmission Switching

PDF: Probability Density Function

RES: Renewable Energy Resources

Vita

Luis D. Ramirez-Burgueno was born in Ciudad Juarez, Chihuahua, Mexico. In December 2020, he received his Bachelor of Science in Electrical and Computer Engineering with a concentration in Power and Energy Systems from the University of Texas at El Paso with cum laude honors. In the Fall of 2019, he joined the Power and Renewable Energy (PRES) Lab. Later, he joined The Powerful Lab as an Undergraduate Research Assistant in the Summer of 2020 under the direction and supervision of Dr. Yuanrui Sang. After finishing his B.S. degree, he began a Master of Science in Electrical Engineering concentrating in Power and Energy Systems while functioning as a Graduate Research Assistant with continued supervision of Dr. Sang. During his master's degree, Luis focused on power system optimization and decentralized algorithms research, which helped to develop a power system resiliency research project along the University of Puerto Rico at Mayagüez sponsored by the National Science Foundation (NSF). During the Spring of 2022, he joined El Paso Electric Company to work in the Real Time Market. Luis is currently an IEEE student member and a Tau Beta Pi Engineering Honors Society member.

Contact Information: ldramirez2@miners.utep.edu, l.ramirezburgueno@gmail.com.